JAERI-M
89-028

STUDY ON POLOIDAL FIELD COIL OPTIMIZATION AND EQUILIBRIUM CONTROL OF ITER

March 1989

Kichiro SHINYA, Masayoshi SUGIHARA and Satoshi NISHIO

日本原子力研究所
Japan Atomic Energy Research Institute

JAERI-M レポートは，日本原子力研究所が不定期に公刊している研究報告書です。
入手の問合わせは，日本原子力研究所技術情報部情報資料課（〒319-11茨城県那珂郡東海村）あて，お申しこしください。なお，このほかに財団法人原子力弘済会資料センター（〒319-11 茨城県那珂郡東海村日本原子力研究所内）で複写による実費頒布をおこなっております。

JAERI-M reports are issued irregularly.
Inquiries about availability of the reports should be addressed to Information Division Department of Technical Information, Japan Atomic Energy Research Institute, Tokai-mura, Naka-gun, Ibaraki-ken 319-11, Japan.

編集兼発行　日本原子力研究所
印　　刷　㈱高野高速印刷

JAERI-M 89-028

Study on Poloidal Field Coil Optimization and Equilibrium Control of ITER

Kichiro SHINYA, Masayoshi SUGIHARA and Satoshi NISHIO

Fusion Experimental Reactor Team
Naka Fusion Research Establishment
Japan Atomic Energy Research Institute
Naka-machi, Naka-gun, Ibaraki-ken

(Received February 7, 1989)

The purpose of this report is to present general features of the poloidal field coil optimization for the ITER plasma, flexibility analysis for various plasma options and some other aspect of the equilibrium control which is required for understanding plasma operation in more detail.

Double null divertor plasma was selected as a main object of the optimization. Single null divertor plasma was assumed to be an alternative, because single null divertor plasma can be operational within the amounts of the total stored energy and ampere-turns of the double null divertor plasma, if it is shaped appropriately.

Plasma parameters used in the present analysis are mainly those employed in the preliminary study by the Basic Device Engineering group of the ITER design team. The most part of the optimization study, however, utilizes the parameters proposed for discussion by the Japan team before starting joint design work at Garching.

Plasma shape, and solenoid coil shape and size, which maximize available flux swing with reasonable amounts of the stored energy and ampere-turns, are discussed. Location and minimum number of the poloidal field coils with adequate shaping controllability were also discussed for various plasma options. Some other aspect of the equilibrium control, such as separatrix swing, moving null point operation during plasma heating and possible range of li, were evaluated and the guideline for the engineering design was proposed. Finally, fusion power output was

estimated for the different pressure profiles and combinations of the average density and temperature, and the magnetic quantities of the scrape-off region was calculated to be available for the future divertor analysis.

Keywords: ITER, Tokamak Reactor, Poloidal Field Coil, Optimization, Equilibrium Control, Divertor Plasma, Separatrix Swing, Moving Null Point Operation, Flexibility, Fusion Power Output

ITERポロイダル系の最適化と平衡制御の検討

那珂研究所核融合実験炉特別チーム
新谷　吉郎・杉原　正芳・西尾　敏

（１９８９年２月７日受理）

本報告はＩＴＥＲポロイダル系の最適化，種々のプラズマ・オプションに対するポロイダル系のフレキシビリティ及び詳細にプラズマ運転を検討する際に必要となる平衡制御に関連した事項を検討した結果をまとめている。

ＩＴＥＲの標準プラズマとしてはダブルヌルダイバータ・プラズマを採用し，シングルヌルダイバータ・プラズマは運転の１オプションとしている。これはシングルヌルダイバータ・プラズマの形状を最適なものに選択すれば，ダブルヌルダイバータ・プラズマに比較してポロイダル系の全蓄積エネルギー，全起磁力のいずれも小さくできることによる。

プラズマ・パラメータとしては西独ガルヒングに於けるＩＴＥＲ設計チームの炉構造技術グループが検討対象とした値を用いているが，ポロイダル系最適化の大部分では共同設計の開始以前に日本チームが予備検討を行った際に使用したものを用いた。

最適化としては出来るだけ少いポロイダル系の蓄積エネルギー及び起磁力で，可能磁束振幅を最大化できるプラズマ形状，ソレノイドコイルの形状及び寸法の検討を中心とした。更にD型プラズマの型状制御を可能とする最小独立コイル数についても検討した。

ダイバータ板への熱負荷を軽減する最適なセパラトリックス・スィング方法，プラズマ加熱時のポロイダル電源容量を過大としないためにヌル点を移動する運転方法についても検討を行った。更に，異ったプラズマ圧力分布や密度と温度の組合せに対して核融合出力を計算し，又，ダイバータ・プラズマに於けるマル点近傍の磁力線構造を求めて，将来のダイバータ・プラズマ解析に資した。

那珂研究所：〒３１１−０１　茨城県那珂郡那珂町大字向山８０１−１

Contents

目　　次

Introduction

The purpose of this report is to present general features of the poloidal field coil optimization for the ITER plasma, flexibility analysis for various plasma options and some aspects of the equilibrium control. Informations about the fusion power and scrape-off layer are also described briefly based on the equilibrium calculations.

Double null divertor plasma is a main object of the optimization. Single null divertor plasma is assumed to be one of the options, because both the total stored energy and ampere-turns are less than those of the double null divertor plasma, if it is shaped appropriately. Plasma parameters used in the present analysis are mainly those employed in the preliminary study by the Basic Device Engineering group of the ITER design team. The most part of the Chapter 1, however, utilizes the parameters proposed for discussion by the Japan team before starting joint design work at Garching.

Usual notations of the plasma parameters are also used in this report. The subscripts M, S, N and 95 denote that the quantities with these subscripts are respectively evaluated at the magnetic axis, plasma surface, null point and the flux surface in which 95 % of the poloidal flux between the magnetic axis and the plasma surface are involved, i.e., $(\Psi-\Psi_M)/(\Psi_S-\Psi_M)=0.95$. Elongation and triangularity of the plasma cross section are evaluated on this flux surface and are represented by κ_{95} and δ_{95}. Elongation is maintained at two throughout the PFC optimization study for the basic plasma, because this value seems to be the highest value for stabilizing the vertical positional instability in ITER, though the stabilization largely depends on the precise reactor structure and the available electric power for the stability control.

Chapter 1 describes the PFC optimization, which mainly includes (1) determination of the preferable plasma shape for operating PFC system with reasonable stored energy and ampere-turns, (2) evaluation of the minimum number of the independent poloidal field coils without deteriorating the shaping controllability of the plasma, and (3) optimization of the sizes of both solenoid and toroidal coils. Chapter 2 briefly describes the results of the equilibrium calculations for various plasma options including single null divertor plasma operation, and the flexibility of the PFC for these operations are also discussed. Chapter 3 is contributed to some other aspect of the equilibrium control which is required to understand the plasma operation in more detail, such as separatrix swing and possible range of l_i.

1. PFC Optimization

Poloidal field coil (PFC) has two main functions, i.e., (1) to supply flux change so that the plasma current are able to ramp up and maintain flat top during plasma burn, and (2) to shape plasma cross section appropriately by separately controlling the dipole, quadrapole, hexapole and, if necessary, octapole magnetic field. The hybrid coil system works as cooperative supply of the above described flux and magnetic fields without separating coils into transformer, vertical coil, etc.

The first function requires rather large number of coils distributed around the plasma to eliminate magnetic field leakage into the plasma region. On the other hand, the second function does not necessarily require so many coils if the adequate shaping control is possible. In this chapter are described the minimum number of the independent coils which is adequately functional for the above two points, the most dominant factor for reducing electric power supply rating, and the influence of the reactor structure emphasizing the aspect of the maintenance access.

1.1 Preferable plasma triangularity

Before starting investigation on obtaining a preferable range of plasma triangularity, brief comparison of the total stored energy and total ampere-turns between double null and single null divertor plasma was carried out to determine which plasma should be selected as a basic plasma for the ITER design. Following plasma parameters were used in the analysis.

$$I_p=20.86 \text{ MA}, \quad R_p/a=5.66/2.05 \text{ m}, \quad \kappa_{95}/\delta_{95}=2.0/0.4.$$

Coil locations are shown in Fig. 1.1-1 and also listed in Table 1.1-1 as a mild oval solenoid. Eighteen coils are distributed around the plasma with up-down symmetry to maximize elimination of the magnetic field leakage into plasma region at initial magnetization.

Figure 1.1-2 shows the effect of the flux difference between active and passive null points, the flux difference being represented by the value of $(\Psi_M-\Psi_{S1})/(\Psi_M-\Psi_{S2})$. Three plasma equilibria for different values of $(\Psi_M-\Psi_{S1})/(\Psi_M-\Psi_{S2})$ are shown in Fig. 1.1-3.

In Fig. 1.1-2 it is seen that a single null divertor plasma with appropriate asymmetry attains minimum total stored energy and has smaller total ampere-turns than a double null divertor plasma. This indicates that the double null divertor plasma should be chosen as a basic plasma for maximizing operation flexibility. The flexibility will be discussed in the next chapter.

Preferable range of plasma triangularity was investigated for three types of solenoid shape, i.e., straight, mild oval and strong oval solenoids. The basic idea of comparing these different solenoid shapes comes from the fact that the straight solenoid has a hump in the ampere-turns distribution near the end of the solenoid at initial magnetization as shown in Fig. 1.1-4. Such hump reduces maximum magnetization flux for the same allowable current density and magnetic field experience of the coils. The total ampere-turns for magnetizing 100 VS in the straight solenoid reaches 170 MAT, while the same value of the magnetization is attained by 149 and 126 MAT for the mild and strong oval solenoids, respectively. Such large total ampere-turns for magnetizing a straight solenoid can of course be reduced by depressing the hump at the sacrifice of increasing magnetic field leakage a little, but the total ampere-turns is still much larger than those of the mild and strong oval solenoids. Depression of the hump in a straight solenoid also increases maximum capability of the magnetization. Figure 1.1-5 depicts the shapes of the solenoids and also plasma equilibria with triangularity of 0.4.

Figure 1.1-6 shows triangularity dependence of (a) maximum total stored energy and (b) available flux swing. At low triangularities, maximum allowable current of No. 7 coil limits the negative end of flux swing. On the contrary maximum magnetic field experience of No. 9 coil limits the flux swing at high triangularities, so there exists a clear break point at moderate triangularity on both the total stored energy and available flux swing curves. The lower value of the available flux swing for the straight solenoid in magnetic-field-limited region corresponds to the existence of the hump in the ampere-turn distribution shown in Fig. 1.1-4.

Generally, triangularity of a plasma cross section can be controlled by push-pull action of the shoulder coil (No.2) and one of the solenoid coils which exists near the null point (No.7). At low triangularity No.7 coil must put the null point outward resulting in requirement of large negative value of ampere-turns at negative end of the flux swing. If the distance between this coil and the null point becomes small, for example, by modifying the solenoid shape oval, less ampere-turns is required for this action, which in turn brings about larger shift to the lower triangularity of the break point for the strong oval solenoid.

The available flux swing attains maximum at the break point, but maximum stored energy does attain minimum at higher triangularity. Ψ_{RAMP} in the Fig. 1.1-6 (b) indicates flux swing required for plasma current ramp-up up to start of plasma burn, so the difference between available flux swing and Ψ_{RAMP}

corresponds to the burn time. Burn time tends to decrease as triangularity increases beyond the break point.

The following figure of merit (FOM) of the poloidal field coil was defined to evaluate a preferable range of triangularity,

$$FOM = \Delta\Psi_p / E_T \quad (VS/GJ).$$

Triangularity dependence of the FOM is shown in Fig. 1.1-7. The FOM reaches maximum at δ_{95}~0.4 for all types of the solenoids. Another figure of merit can be defined by

$$FOM = \Delta\Psi_p / \Sigma|I_{MAX}| \quad (VS/MAT),$$

where I_{MAX} is the maximum ampere-turns in absolute sense during overall operation period. $\Sigma |I_{MAX}|$ has a similar triangularity dependence as $\Delta\Psi_P$ as shown in Fig. 1.1-8, so the FOM has rather flat profile which is shown in Fig. 1.1-9.

Both FOMs indicate advantages in designing PFC with oval solenoid and selecting plasma triangularity of about 0.4. The PFC optimization study was carried out at δ_{95} of 0.4 with mild oval solenoid hereafter in Chapter 1. It should be noted that the final selection of the solenoid shape must await the result of the investigation on the reactor structure and maintenance.

1.2 Number of independent coil

As a starting point of PFC optimization, a distributed PFC, which is shown in Fig. 1.1-1, was selected. Optimization was carried out in such a way of eliminating a particular coil or connecting neighbouring coils in series to reduce the number of independent coils. All the solenoid coils can be connected in series if only current transformer function is to be realized, but in hybrid coil system some freedom in the solenoid coil is required for especially controlling triangularity.

At the beginning was tried series connection of the three nearest coils to the median plane (No. 7, 8 and 9). Figure 1.2-1 depicts the effect of series connection. Series connection of No. 8 and 9 coils does not alter ampere-turns distribution so much at least for a plasma with triangularity of 0.4. Three-coil series connection almost doubles the ampere-turns of the neighbouring No. 6 coil in the opposite direction. This effect in turn propagates up to the top coil (No. 3). Such large amplitude oscillation of the ampere-turns distribution increases the total ampere-turns, otherwise deteriorates controllability of a plasma shape because of fixed pattern of pushing force by solenoid coils. It might also be concluded that No. 5 and 6 coils can be connected in series to

further reduce the number of independent coils. This point will be discussed in the next paragraph by comparing ampere-turns distributions for different poloidal beta values and linkage fluxes.

Figure 1.2-2 shows ampere-turns distributions of 2-coil series connection for three different particular times of operation, i.e., (a) before heating (BH), (b) start of burn (SOB) and (c) end of burn (EOB). Three triangularities were studied to simulate separatrix swing. The figure indicates a possibility of connecting No. 5 and 6 coils in series in the triangularity range of 0.3-0.5. It should be noted that the final decision of series connection must await the result of the precise investigation on the reactor structure and electric power supply same as for the solenoid shape.

In the following the effect of eliminating a particular coil will be discussed with taking a maintenance access into consideration. For the first step the top coil in Fig. 1.1-1 was eliminated to simulate vertical access for the maintenance. Figure 1.2-3 depicts triangularity dependence of (a) total stored energy and (b) available flux swing together with the dependence for the original coil arrangement. There exists no meaningful difference between them in the practical range of triangularity. The top coil can therefore be eliminated from the ITER PFC system. The figure of merit is shown in Fig. 1.2-4 where preferable triangularity range still remains around 0.4.

Ampere-turns distribution was examined to see in detail the effect of eliminating the top coil. The results are shown in Fig. 1.2-5. It is worth noting that coils are numbered without the top coil in this figure and that No. 8 and 9 coils are connected in series. Although the macroscopic quantities such as the total stored energy and the total ampere-turns remain almost unchanged, the ampere-turns of the divertor coil (No. 4 in Fig. 1.2-2 and No. 3 in Fig. 1.2-5) almost doubles without the top coil, the value corresponding to the sum of the divertor and top coils. The ampere-turns of the shoulder coil also tends to increase without the top coil.

Further elimination of the shoulder coil is attractive to complete the vertical access for the maintenance, though the ampere-turns of the residual coils seem to increase significantly. Figure 1.2-6 shows the ampere-turns distribution without the top and shoulder coils. It should be noted again that coils are renumbered in the figure, and that shaping plasma highly triangular (>0.4) becomes difficult due to lack of independent supply of the quadrapole and hexapole magnetic fields which is effectively done by the shoulder and outermost coils.

Significant feature of the coil arrangement without the shoulder coil is characterized by the followings.

(1) The ampere-turns of the divertor coil (No. 2) becomes negative.
(2) The ampere-turns of the two neighbouring coils (No. 3 and 4) which exist at the end of the solenoid increase quite much to compensate the negative ampere-turns of the divertor coil.
(3) Controllability of the triangularity and separatrix shaping deteriorates.

It can therefore be concluded that at least two independent coils are required for adequate control of plasma shape at the outer region of the reactor structure.

In order to simulate horizontal access for the maintenance, elimination of the outermost coil was examined. Figure 1.2-7 shows stored energy distributions with and without the outermost coil. Though the shaping ability is not so deteriorated as in the case of eliminating the shoulder coil, stored energy of the shoulder and the top coils remarkably increase up to unrealistic level. Because the stored energy of such isolated coil with large bore is dominated by the contribution from self-inductance, it can somewhat be reduced by expanding cross section of the coil. However reduction to an appropriate level, for example 2 GJ, does not seem to be compatible with reactor structure due to logarithmic dependence of the self-inductance on the cross section of the coil. Based on the above results, vertical access for the maintenance is much more advantageous than horizontal access to reduce the PFC system quantities for the ITER plasma with high elongation of about 2.

In conclusion, at least six independent coils are required for controlling plasma shape adequately within reasonable values of ampere-turns and stored energy of the coil. Detail of the minimum number of the independent coils is 3 for the solenoid, 1 for the divertor and 2 for outside the major radius of the plasma.

1.3 Location of shoulder coil

Usually shoulder coil is accompanied with large ampere-turns and stored energy, especially, at high triangularity and low poloidal beta. This is mainly due to requirement of the large hexapole magnetic field for triangular shaping of the plasma cross section. As the hexapole field decreases as d^{-2}, where d is a distance from the coil, the shoulder coil should be located as close as possible to the plasma. In the following, ampere-turns and stored energy distributions are investigated for two locations of the shoulder coil. Basic coil locations are shown in Fig. 1.3-1. These locations are fully compatible with maintenance access, i.e., straight solenoid to be easily pulled out and large top and bottom access area by eliminating the top coil and shifting the shoulder

coil outside to the same major radius as the outermost coil. Table 1.3-1 summarizes the coil locations and sizes.

As is confirmed in Figs. 1.3-2 and 1.3-3, reducing major radius of the shoulder coil from 11.5 m to 9.8 m decreases the ampere-turns and the associated stored energy of the shoulder coil without changing ampere-turns of the solenoid and divertor coils. The ampere-turns of the outermost coil changes so as to keep vertical field constant. Reduction of the total stored energy is significant in low β_p plasma (shown as Before Heating) due to higher hexapole field requirement for the same plasma cross section shape compared with high β_p plasma. If the distant shoulder coil is inevitable for the maintenance access and reduction of the electric power is greatly desirable, triangularity of the plasma cross section at low β_p should be decreased to mitigate hexapole field requirement. This idea of plasma operation will be described in section 3.2.

1.4 Solenoid coil optimization for magnetization flux capability

When the PFC system provides the initial magnetization flux to a plasma column, the flux value depends on only the solenoid coil design, and the function of the other PF coils (the so-called ring coils) is confined to reduce a stray field in the plasma region. Therefore investigation was focused on the solenoid coil design in evaluating the obtainable magnetization flux.

A forced-flow cooling of cable-in-conduit conductors was employed for the solenoid coil. The schematic picture of material fraction in the conductor unit is shown in Fig.1.4-1. As a basic design consideration, the helium void fraction in the cable region ($f_{He}=\gamma_{He}/\gamma_{cable}$) was fixed to be 0.4, based on the manufacturing experience of the cable-in-conduit conductor. This value seems to be a minimum value in order to avoid the severe critical current degradation during the manufacturing process. The fraction of copper in conductor strand region ($f_{cu}=\gamma_{cu}/\gamma_{st}$) was chosen to be 0.6 in order to satisfy the protection requirements in the occurrence of a quench. The quantity of the supper conductor (γ_{sc}) was designed based on not only the critical current density which is function of the magnetic field strength, but also the required temperature margin of the conductor. Thus as shown in Fig. 1.4-2, was obtained a design curve which indicates the set of the allowable magnetic field and current density in the cable region. In addition, the solenoid coil should be designed to be self-supporting system against the electromagnetic hoop force. This force is supported by the stainless steel conduit ($\gamma_{conduit}$). The cross sectional area of stainless steel conduit was chosen so that the average tensile stress over the winding-pack cross section

is less than 500 MPa. The fraction of the insulation and the dead space (γ_I) was assumed to be 0.1.

According to the above mentioned design conditions, the obtainable magnetization flux, which corresponds to an arbitrary design point in Fig. 1.4-2, can be evaluated as a function of the thickness of solenoid coil under a certain outer bore of solenoid coil. Figure 1.4-3 is an example in the case of the solenoid coil outer radius of 1.765m. Each design point in Fig. 1.4-2 has its optimum coil thickness, where the obtainable magnetization flux is maximized. In Fig. 1.4-3, the left side of optimum point is limited by the constraints of current density and tensile stress, while the right side is limited by the maximum allowable magnetic field. By smoothly connecting the maximum points and then making an envelope curve, the maximum obtainable magnetization flux was obtained as a function of the design magnetic field for the several kinds of coil outer bore as shown in Fig. 1.4-4. The optimum design magnetic field depends on the coil outer bore. Finally, the dependence of maximum obtainable magnetization flux on the coil radius (half of outer bore) is shown in Fig. 1.4-5, and this tendency is close to a parabolic curve.

1.5 Effect of toroidal coil bore size on field ripple and PFC capacity

Bore size of toroidal coils is determined by the physics specification of the field ripple at the outer plasma edge and by the choice of the number of toroidal coils. It is also affected by the use of ferromagnetic insert to reduce the field ripple. The capacity of poloidal field coil system is greatly affected by the bore size of TF coils. Thus, it is of primary importance to clarify quantitatively relations among bore size, number of TF coil, ripple value and the capacity of PF system for establishing the design concept. Figure 1.5-1 shows the toroidal field ripple at the plasma edge δ_0 as a function of the position of TF outer leg (center of conductor) for three cases of TF coil number N (N=12, 14 and 16). Position of plasma outer surface (separatrix) at the midplane is 7.69 m and the thickness of TF coil conductor is 0.3 m. Dotted lines show the ripple value when the magnetic insert is used for each TF coil number case. Width, thickness and height of the insert are assumed 0.6m x 0.6m x 5.25m for all cases. Configuration of the insert is shown in Fig. 1.5-2. Generally, ferromagnetic inserts under the TF coils can reduce the ripple level and have the equivalent effect to increase the number of TF coil by 2. In Fig. 1.5-1 is also shown the total stored circuit energy of poloidal coil system E_S at the end of burn state. Poloidal coils are distributed uniformly along the TF coils in the calculation of E_S. It decreases linearly as the bore size decreases, while the degree of this reduction is weakened as the position of TF outer leg

decreases below about 10.5 m, because the total system energy is dominated by the solenoid and divertor coils for such small TF bore size.

Table 1.1-1 Coil locations for three different solenoids

	Straight		Mild Oval		Strong Oval	
	R	Z	R	Z	R	Z
1	11.4	3.1	11.4	3.1	11.4	3.1
2	9.8	6.0	9.8	6.0	9.8	6.0
3	6.8	8.2	6.8	8.2	6.8	8.2
4	4.15	8.35	4.15	8.35	4.15	8.35
5	2.15	7.2	2.4	7.2	2.95	7.2
6	1.55	5.6	1.9	5.6	2.2	5.6
7	1.55	4.0	1.65	4.0	1.85	4.0
8	1.55	2.4	1.57	2.4	1.7	2.4
9	1.55	0.8	1.55	0.8	1.55	0.8

Table 1.3-1 Coil locations and sizes

	R(m)	Z(m)	ΔR(m)	ΔZ(m)
PF1a	1.67	0.8	0.6	1.4
1b	1.67	2.4	0.6	1.4
2	1.67	4.0	0.6	1.4
3a	1.67	5.6	0.6	1.4
3b	1.67	7.2	0.6	1.4
4	4.15	8.35	0.6	1.0
5	11.5	6.2	0.8	0.8
6	11.5	3.1	0.8	0.8

Coils are located with up-down symmetry.

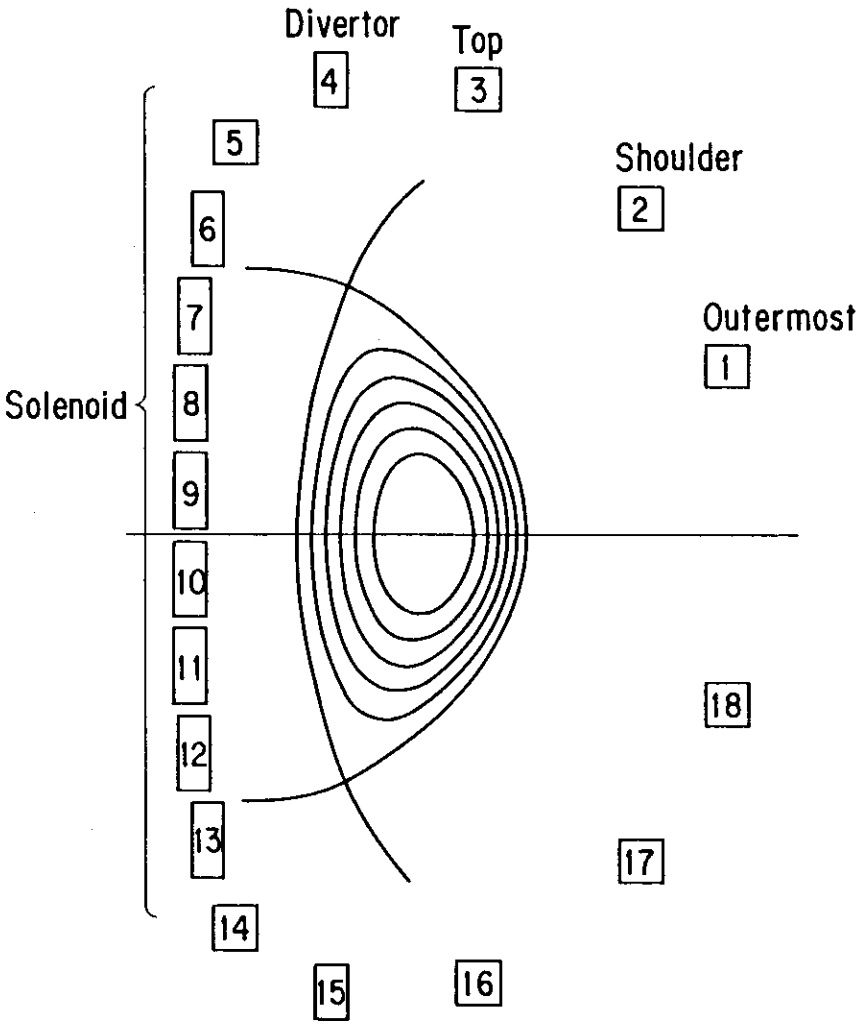

Fig. 1.1-1 Coil locations and notations for studying effects of the plasma triangularity, solenoid shape, series connection of the solenoid coils and maintenance accesses.

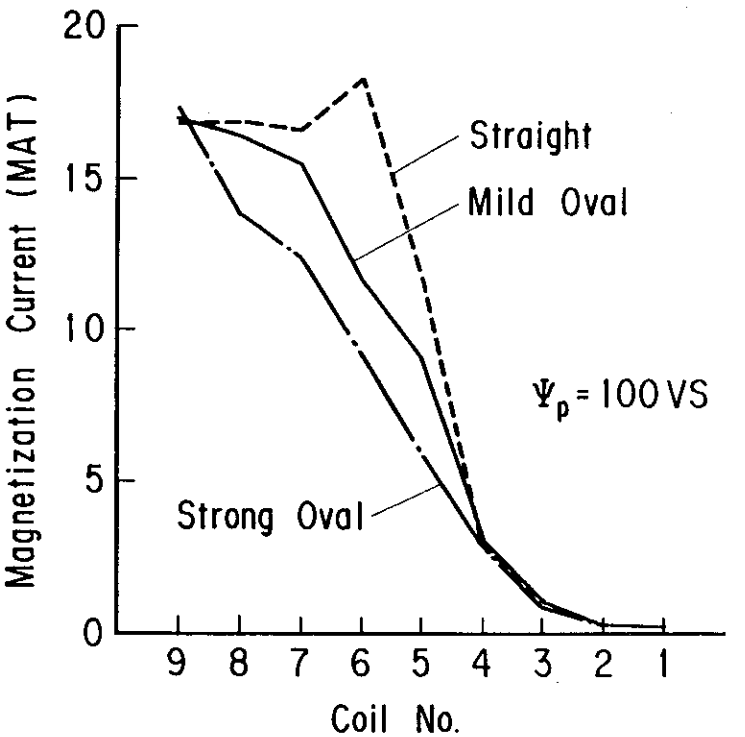

Fig. 1.1-4 Ampere-turns distributions for straight, mild oval and strong oval solenoids. A hump exists near the end of the solenoid in the straight solenoid poloidal coils.

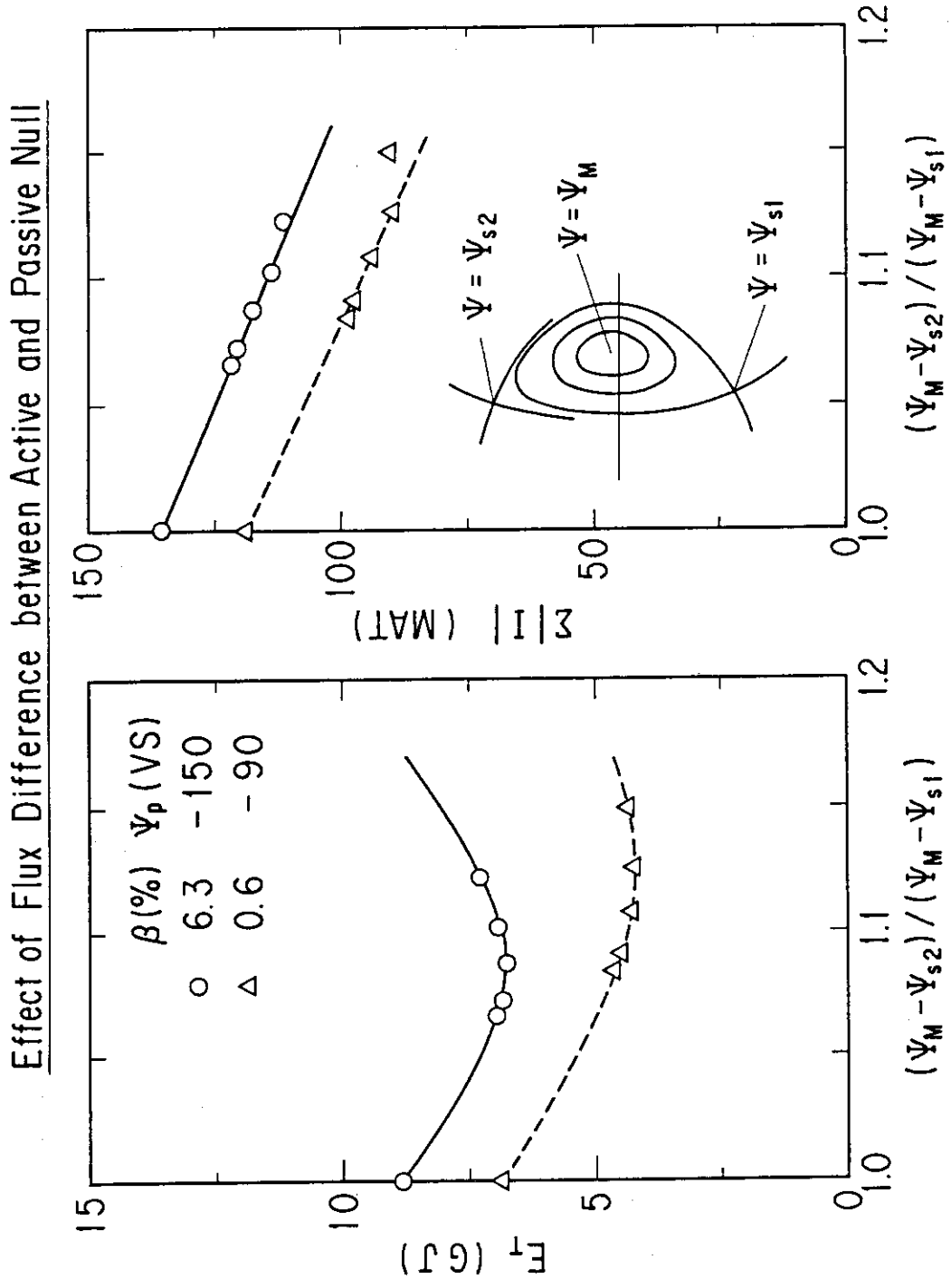

Fig. 1.1-2 Effect of the flux difference between active and passive nulls on the total stored energy and total ampere-turns. Single null plasma with appropriate updown asymmetry has the minimum stored energy.

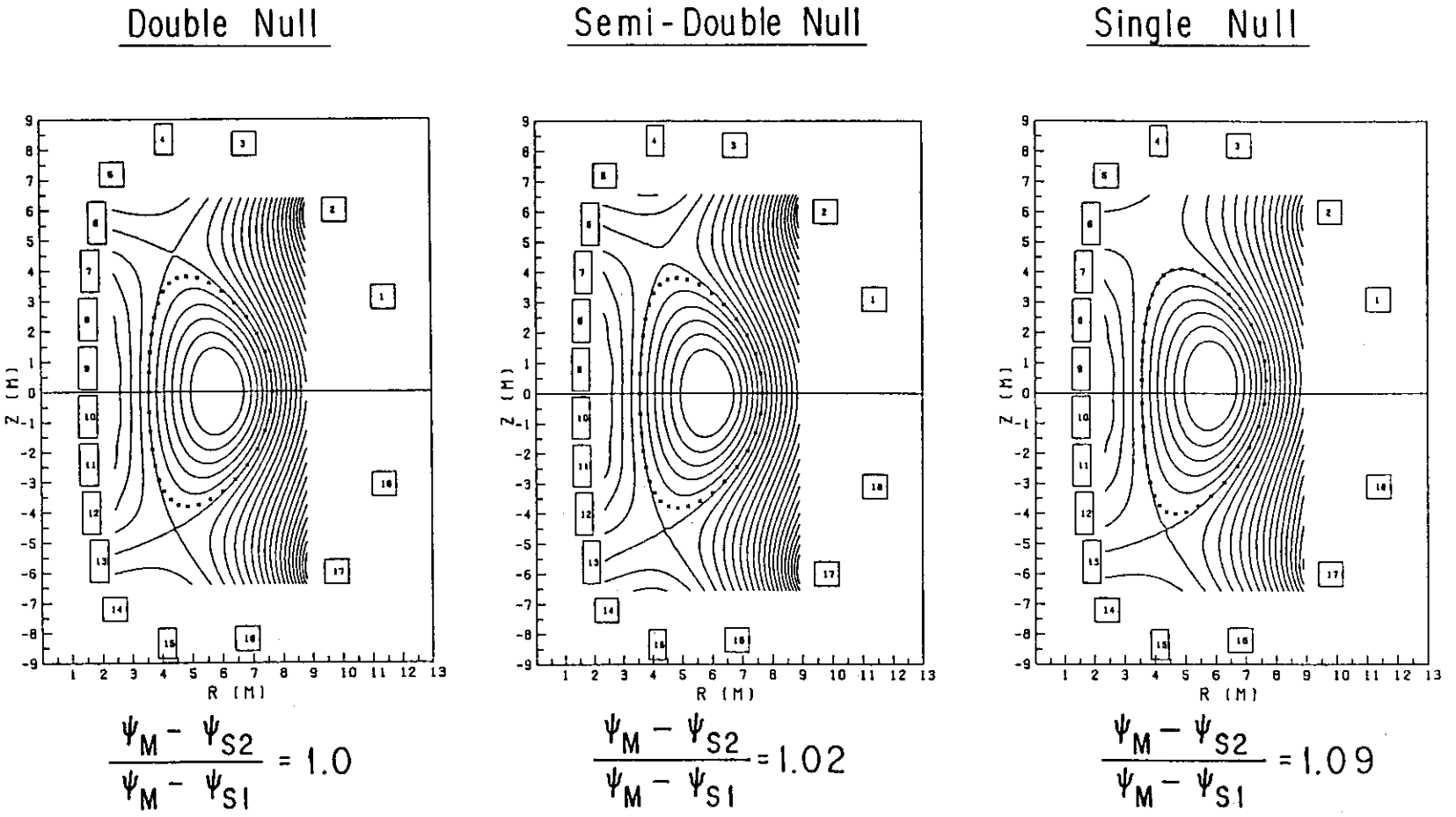

Fig. 1.1-3 Typical plasma equilibria with different degree of up-down asymmetry.

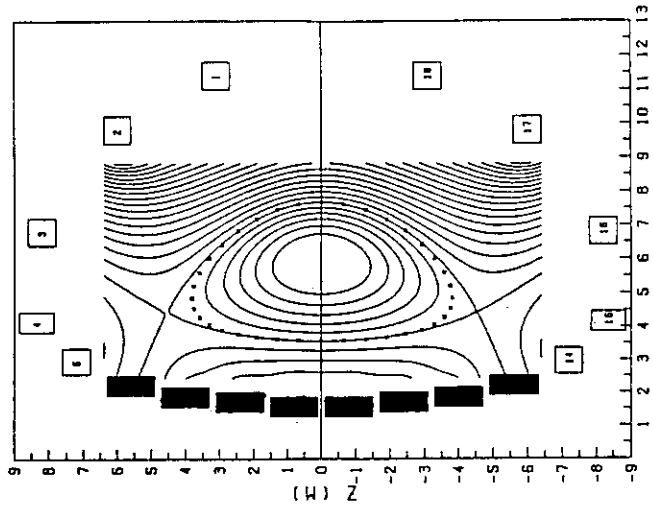

(c) Strong Oval Solenoid

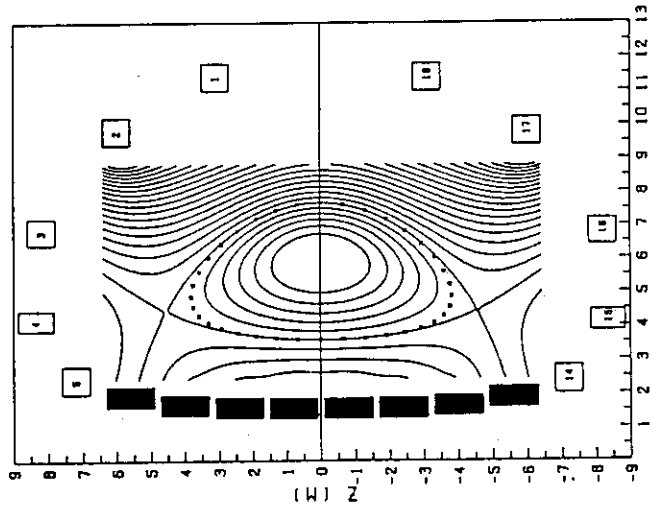

(b) Mild Oval Solenoid

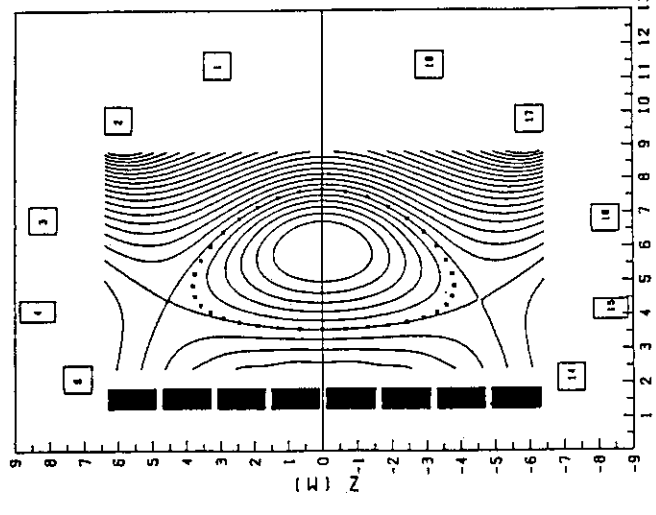

(a) Straight Solenoid

Fig. 1.1-5 Solenoid shapes.

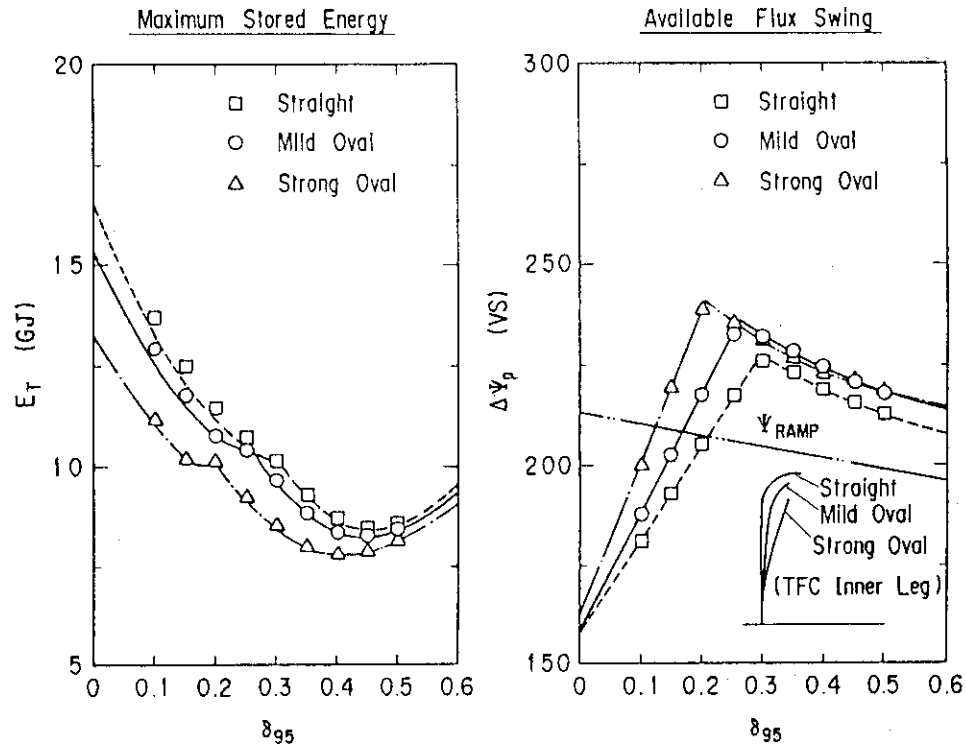

Fig. 1.1-6 Triangularity dependence of the total stored energy and available flux swing. The break point corresponds to the transition point from current density limited region to magnetic field limited region of the solenoid coils.

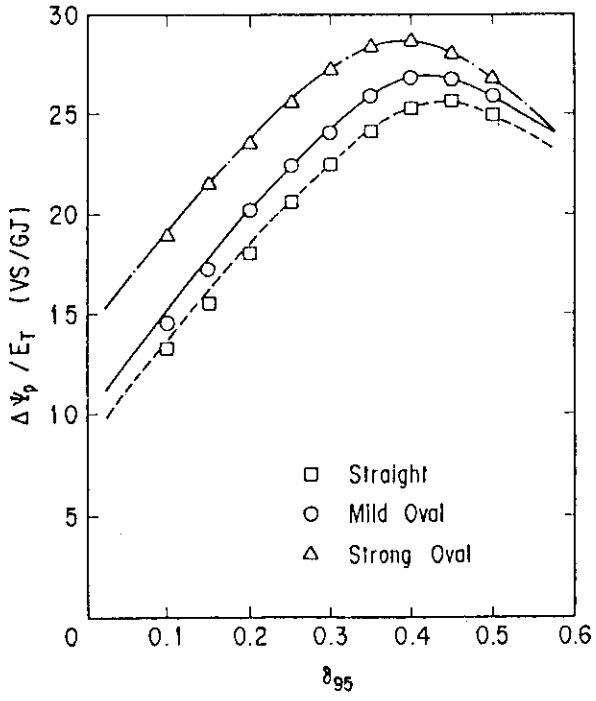

Fig. 1.1-7 Figure of merit of the poloidal field coil system defined by the available flux swing per unit stored energy.

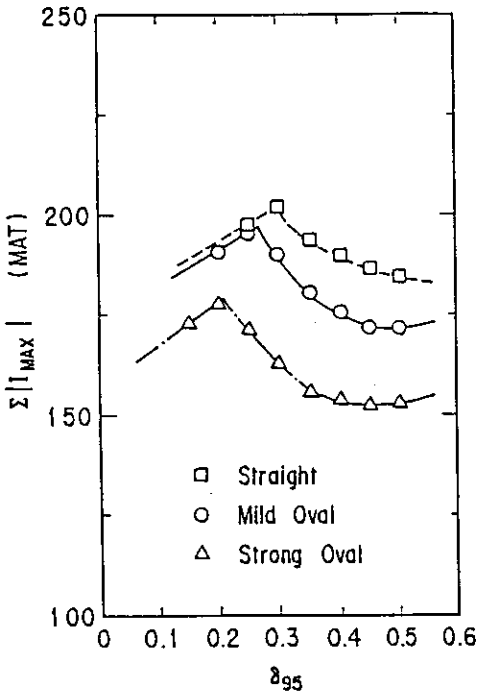

Fig. 1.1-8

Triangularity dependence of the total ampere-turns.

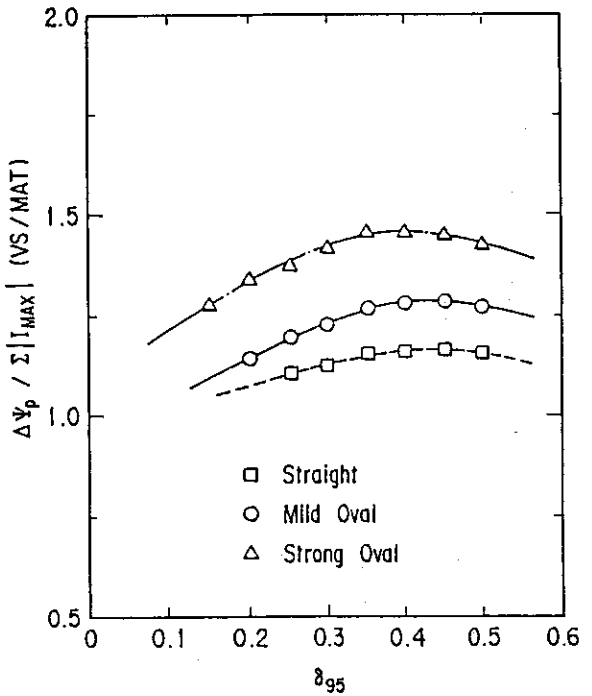

Fig. 1.1-9

Figure of merit defined by available flux swing per unit total ampere-turns. This definition of the FOM shows rather flat profile for the change in the triangularity.

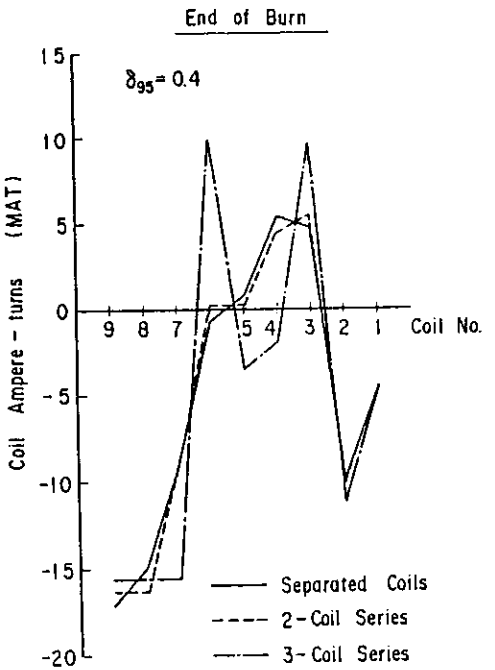

Fig. 1.2-1

Effect of the series connection on the ampere-turns distribution. Series connection of the neighbouring three coils near the midplane does change the distribution significantly.

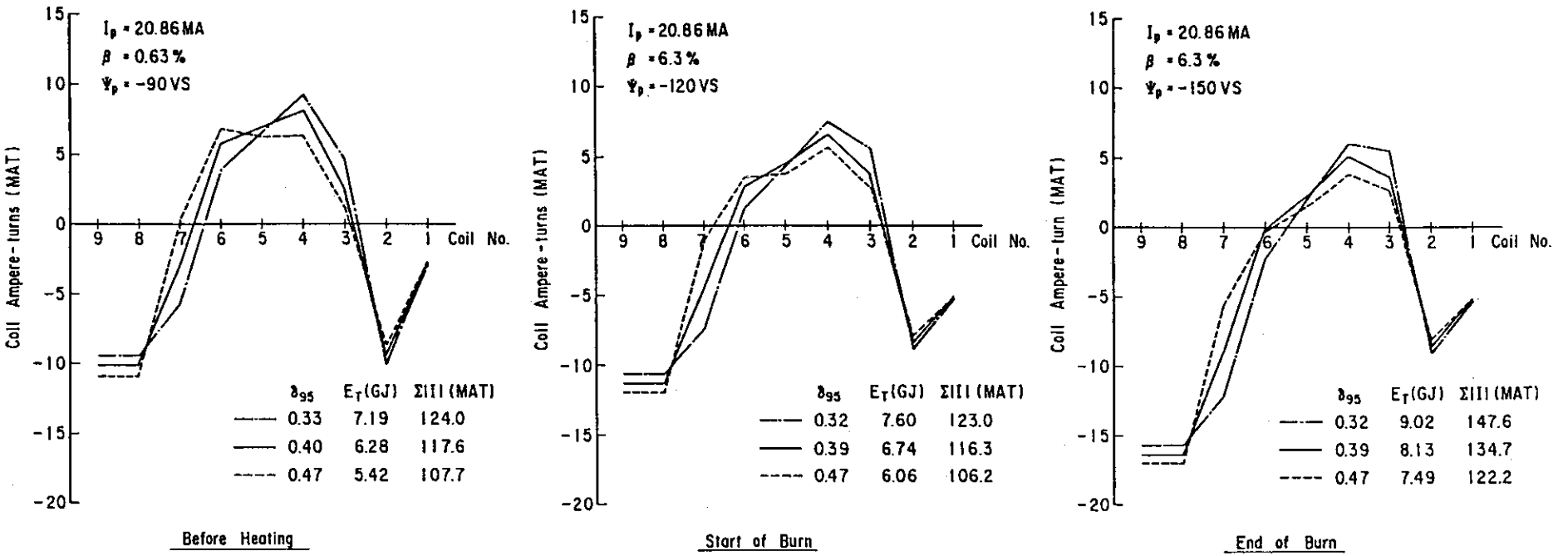

Fig. 1.2-2 Ampere-turns distributions for different triangularities. Triangularity can easily be controlled by slight change in ampere-turns of the coils. Note that the solenoid shape is mildly oval and two coils near the mid plane are connected in series.

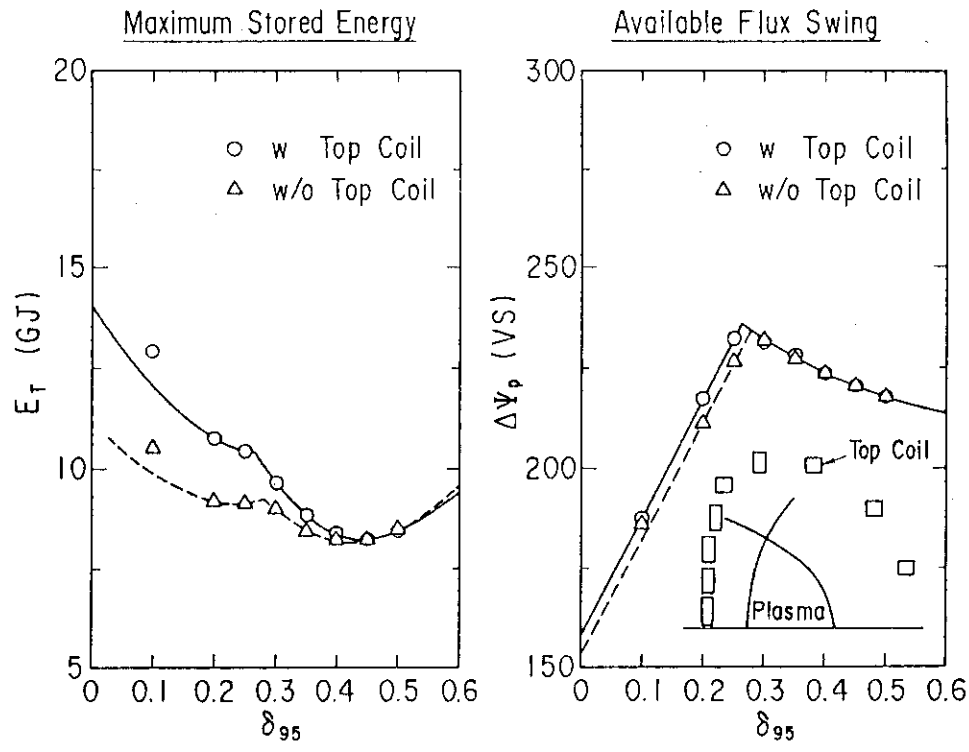

Fig. 1.2-3 Triangularity dependence of the total stored energy and available flux swing for PFCs with and without the top coil. Elimination of the top coil hardly affects both dependences in the preferable triangularity region around 0.4.

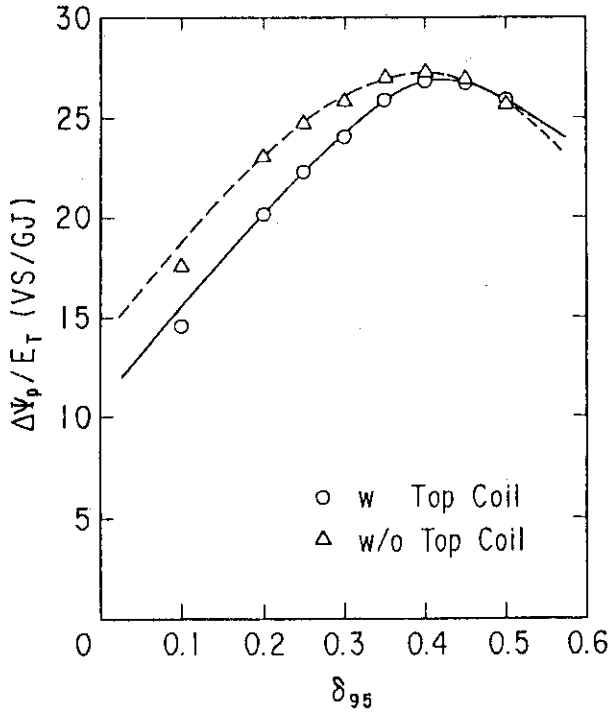

Fig. 1.2-4 FOMs for PFCs with and without the top coil.

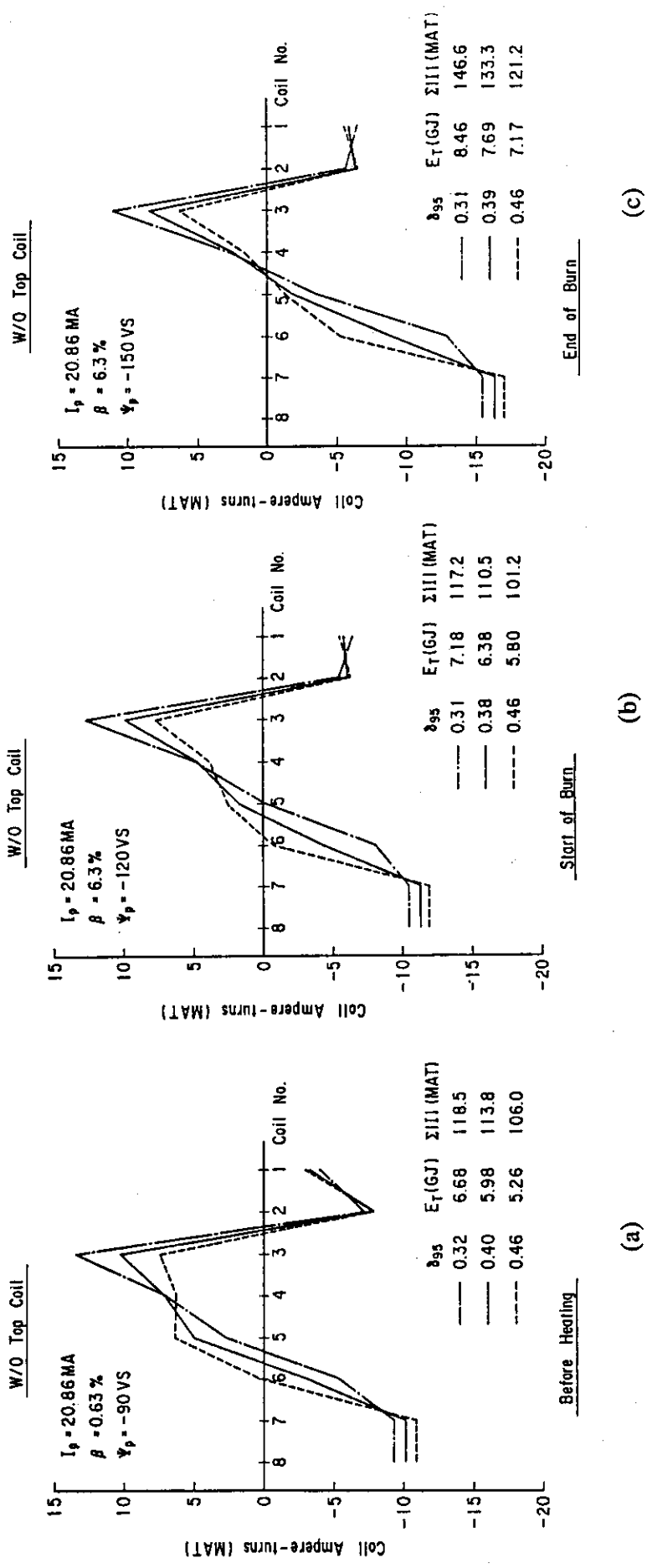

Fig. 1.2-5 Ampere-turns distributions for PFC without the top coil. The divertor coil has more increased amperetums than the PFC with the top coil.

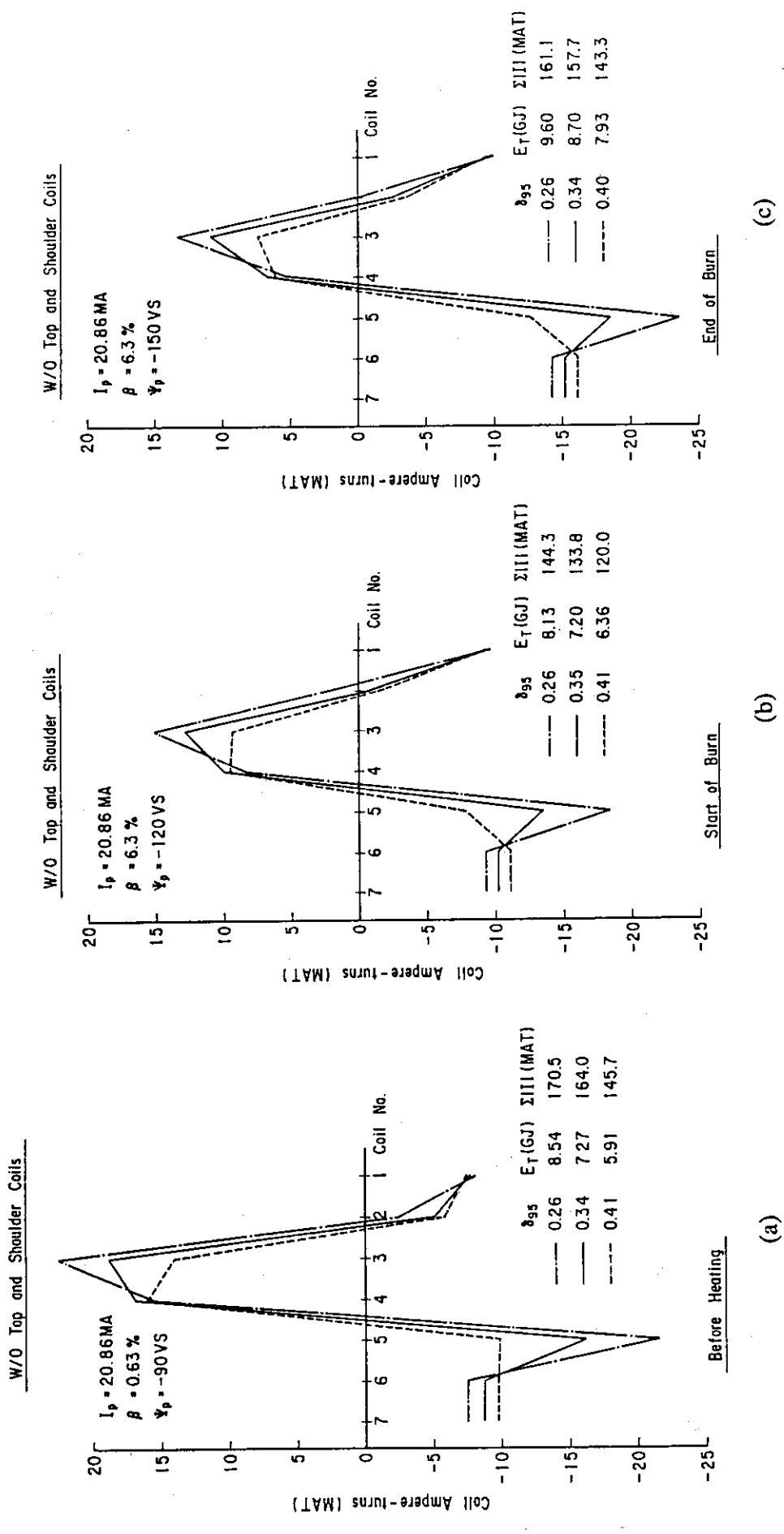

Fig. 1.2-6 Ampere-turns distributions without the top and shoulder coils. Simultaneous elimination of the top and shoulder coils increases coil ampere-turns significantly.

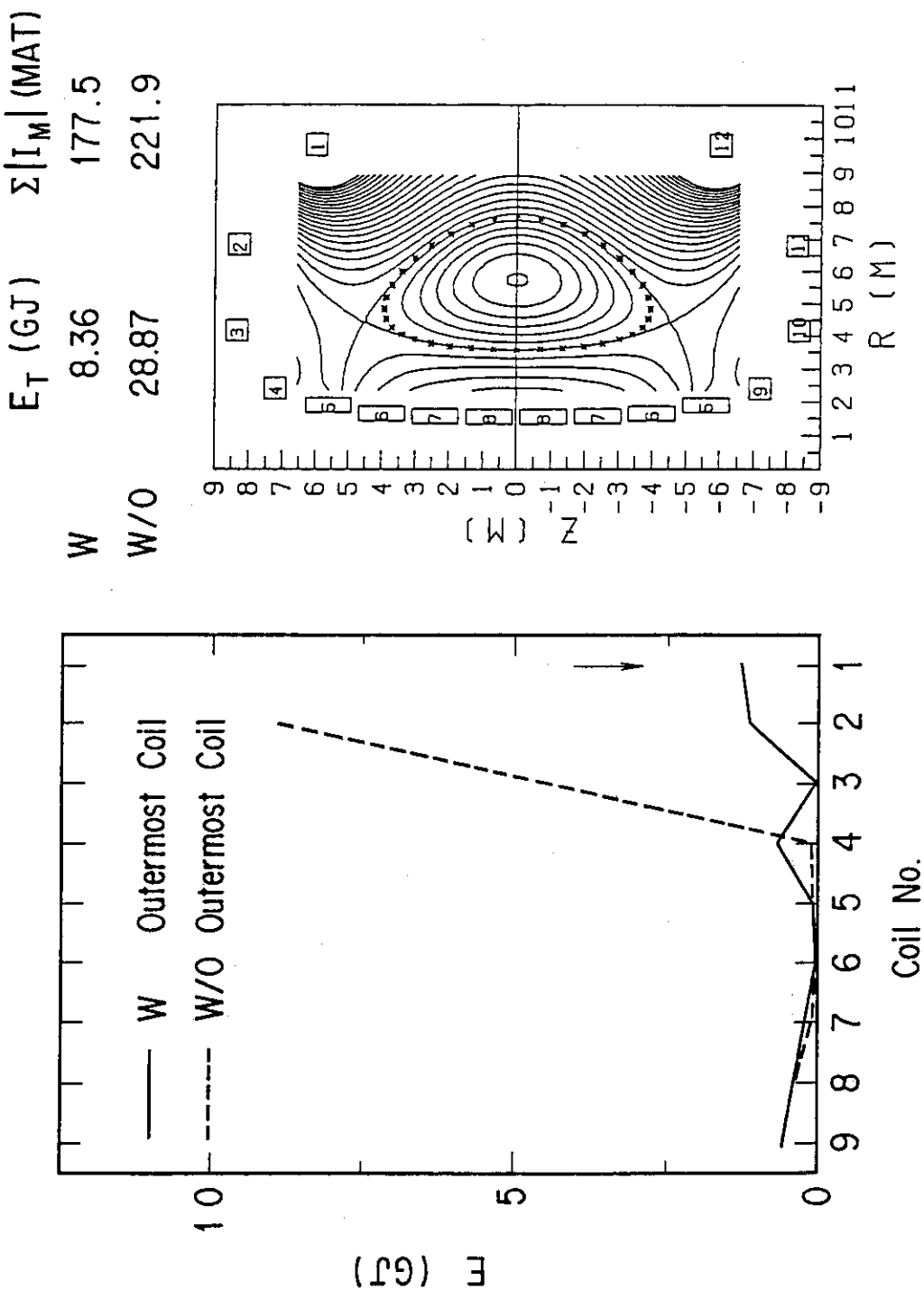

Fig. 1.2-7 Stored energy distribution for PFCs with and without the outermost coil. Elimination of the outermost coil significantly increases stored energy of the shoulder coil, though the plasma shaping is easily done for the ITER plasma parameters.

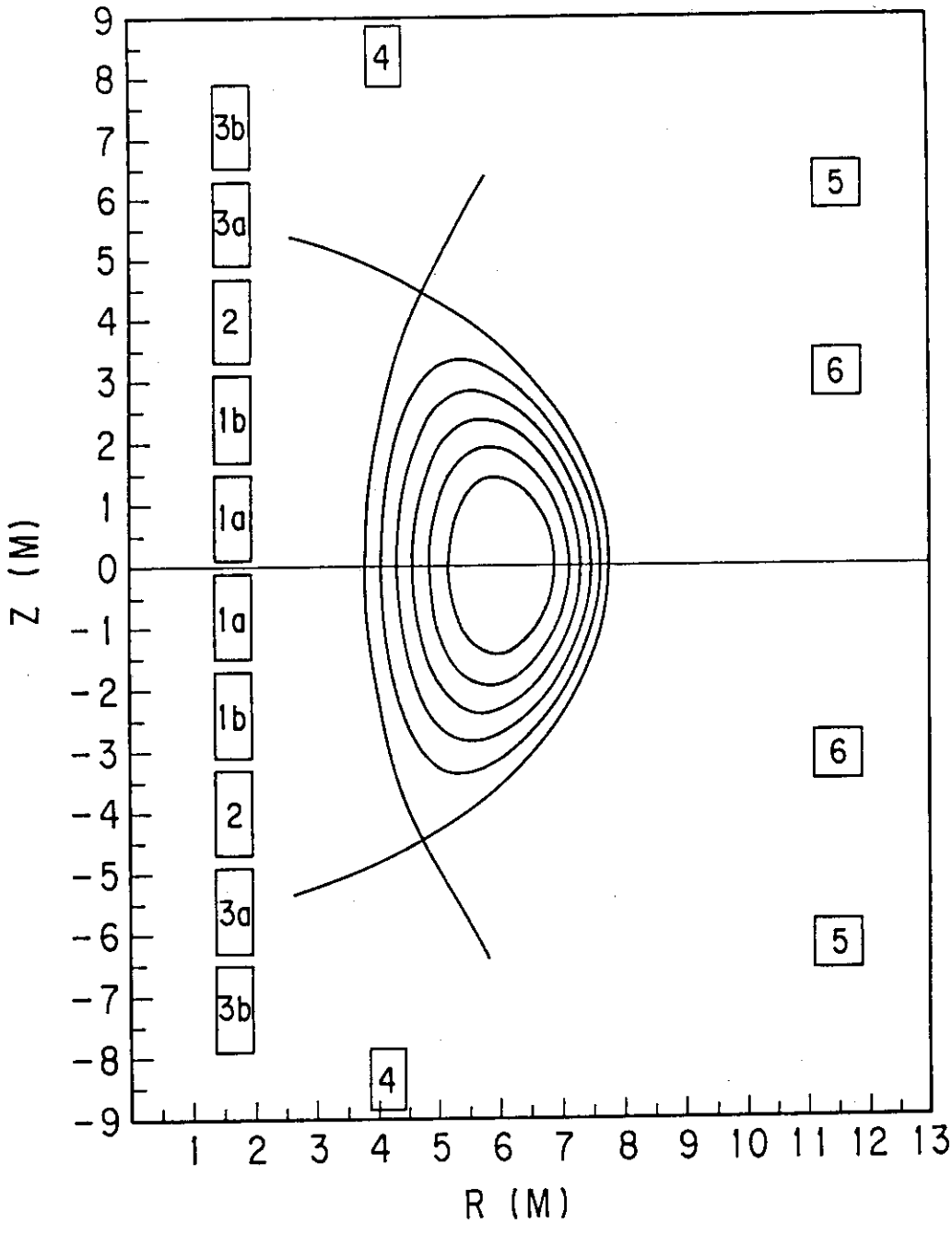

Fig. 1.3-1 Reference coil locations with maintenance access viewpoint largely included.

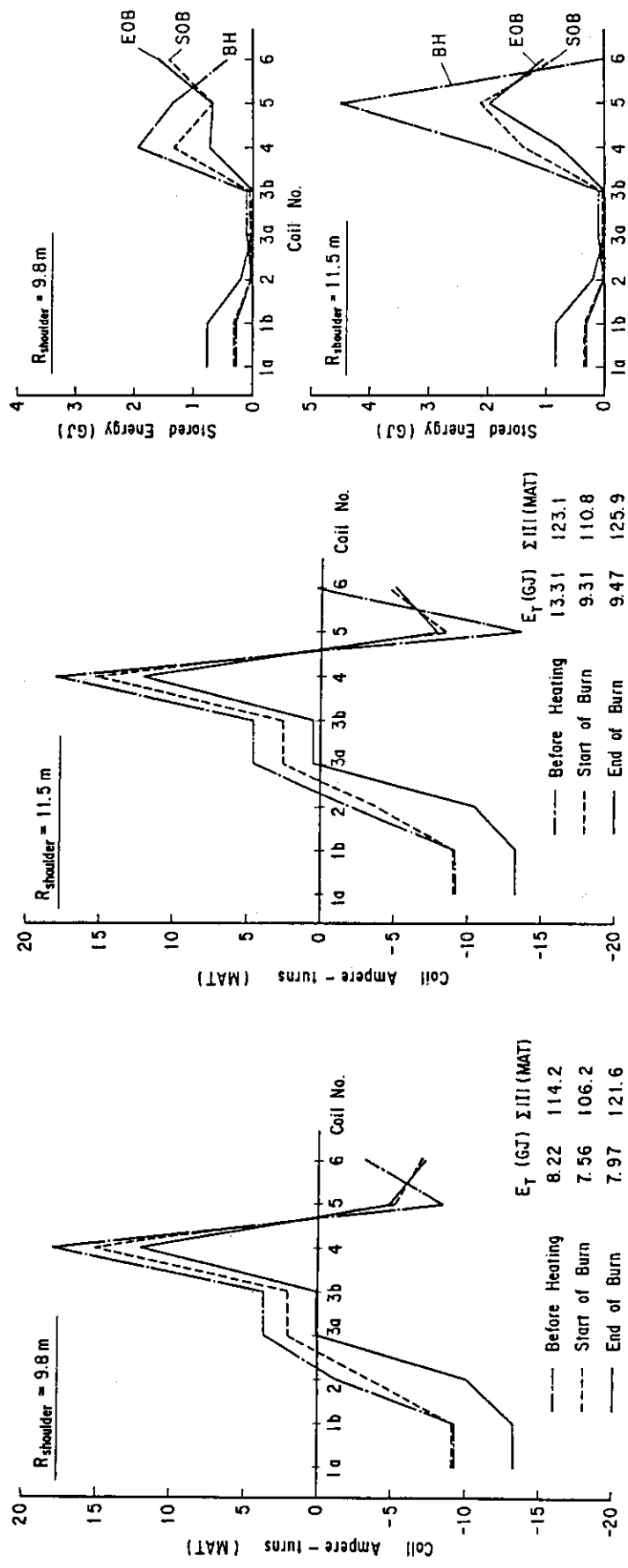

Fig. 1.3-2 (a)

Fig. 1.3-2 (b)

Fig. 1.3-3

Fig. 1.3-2 Comparison of the ampere-turns distribution between (a) decreased radius shoulder coil and (b) reference shoulder coil.

Fig. 1.3-3 Comparison of the stored energy distribution between two cases of the shoulder coil. The stored energy in the shoulder coil of the reduced major radius significantly decreases associated with decrease of its ampere-turns.

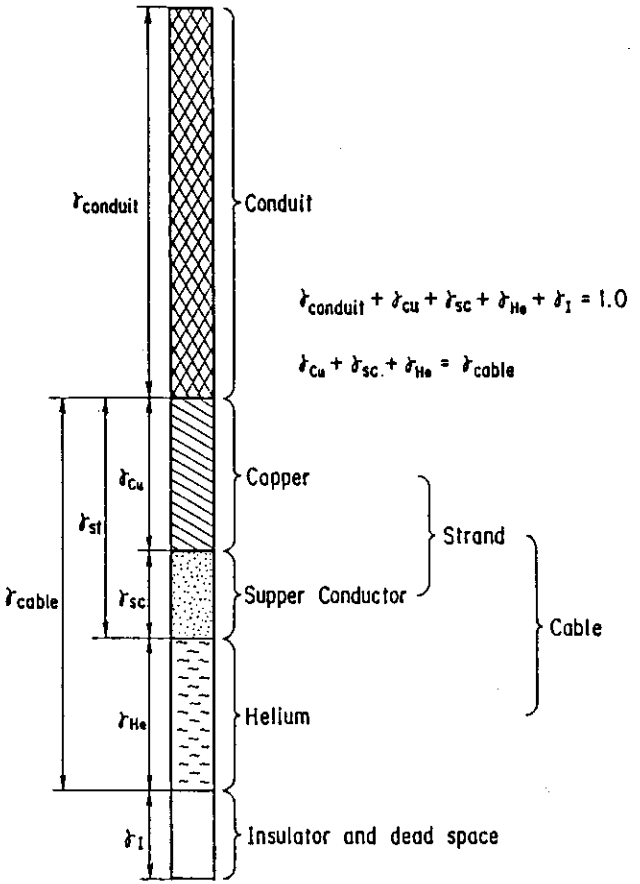

Schematic picture of PFC conductor unit

Fig. 1.4-1 Schematic picture of cable-in-conduit type PFC conductor unit.

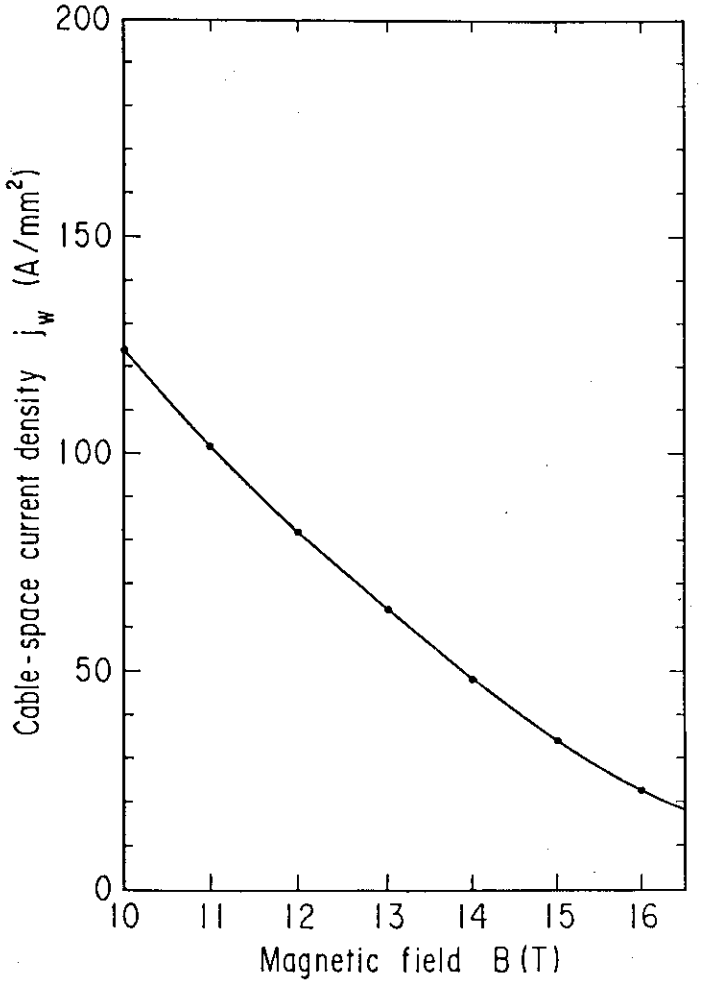

Cable-space current density for PF coils

Fig. 1.4-2 Magnetic field dependence of the critical current density averaged over the cable-space cross section.

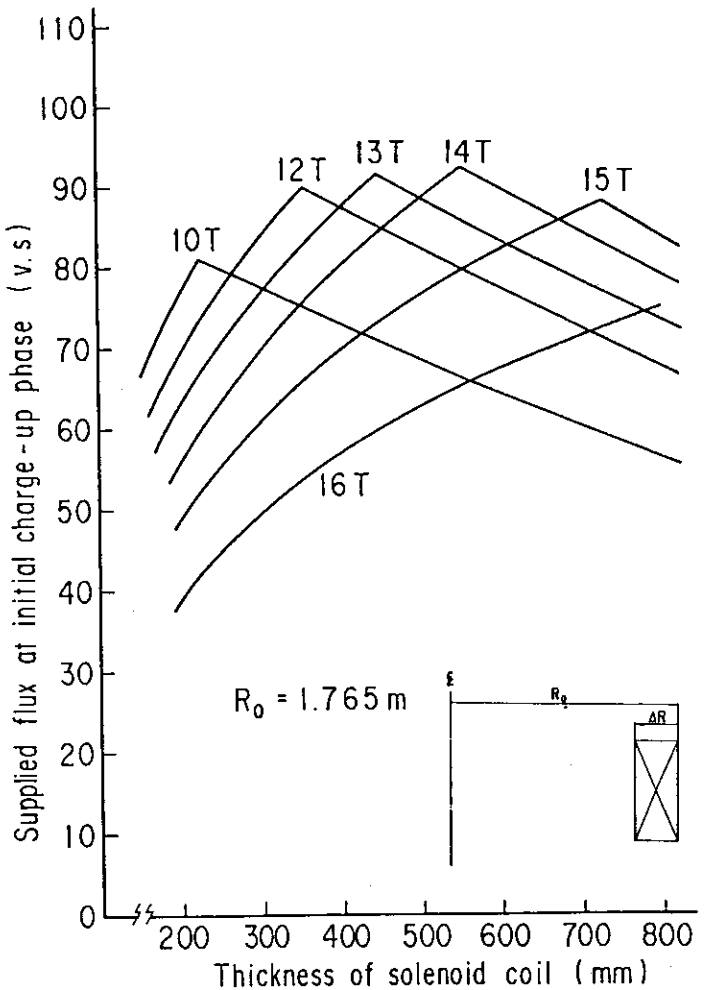

Fig. 1.4-3 Dependence of the maximum initial magnetization flux on the thickness of the solenoid coil with fixed value of the solenoid coil outer radius (R_0=1.765 m).

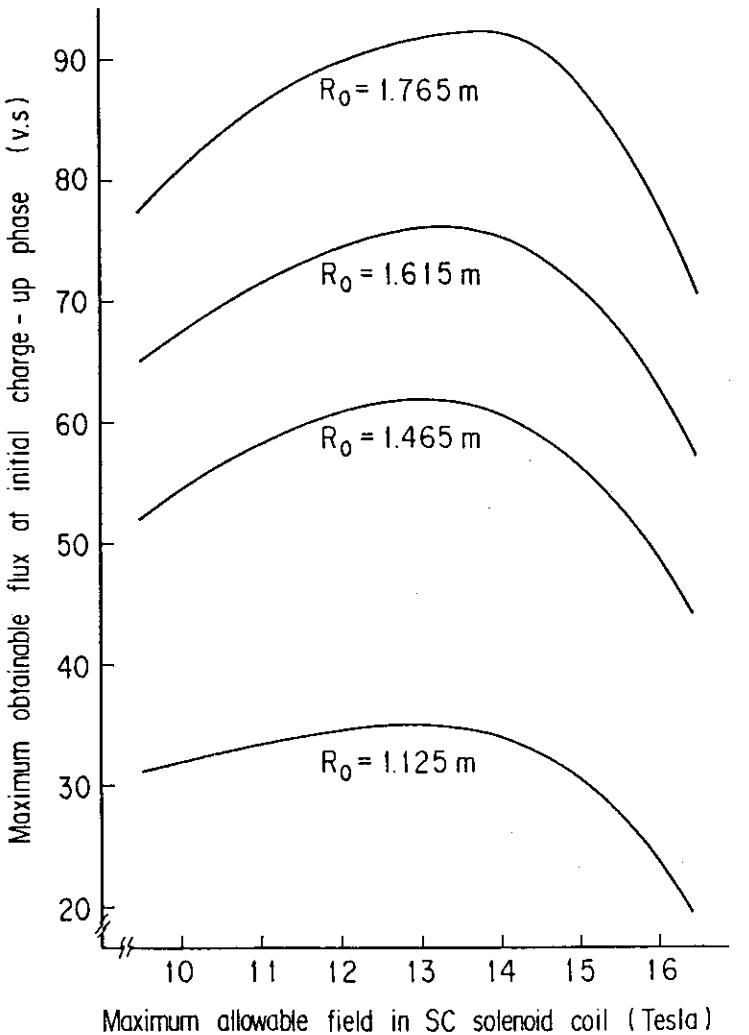

Fig. 1.4-4 Dependence of the maximum obtainable initial magnetization flux on the maximum allowable magnetic field in the SC solenoid coil for different values of the solenoid coil outer radius.

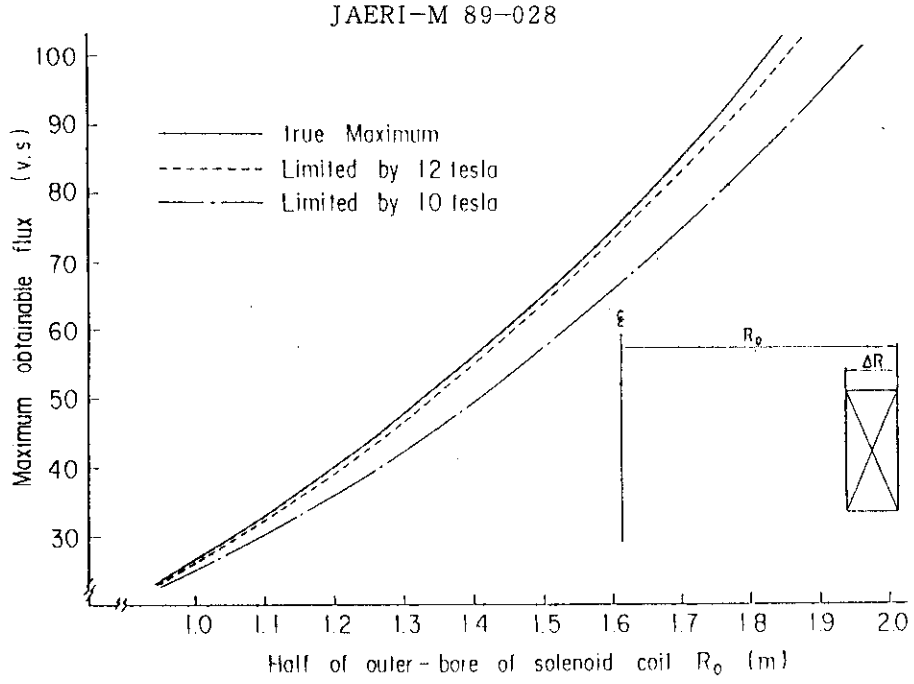

Fig. 1.4-5 Dependence of the maximum obtainable initial magnetization flux on the solenoid coil outer radius.

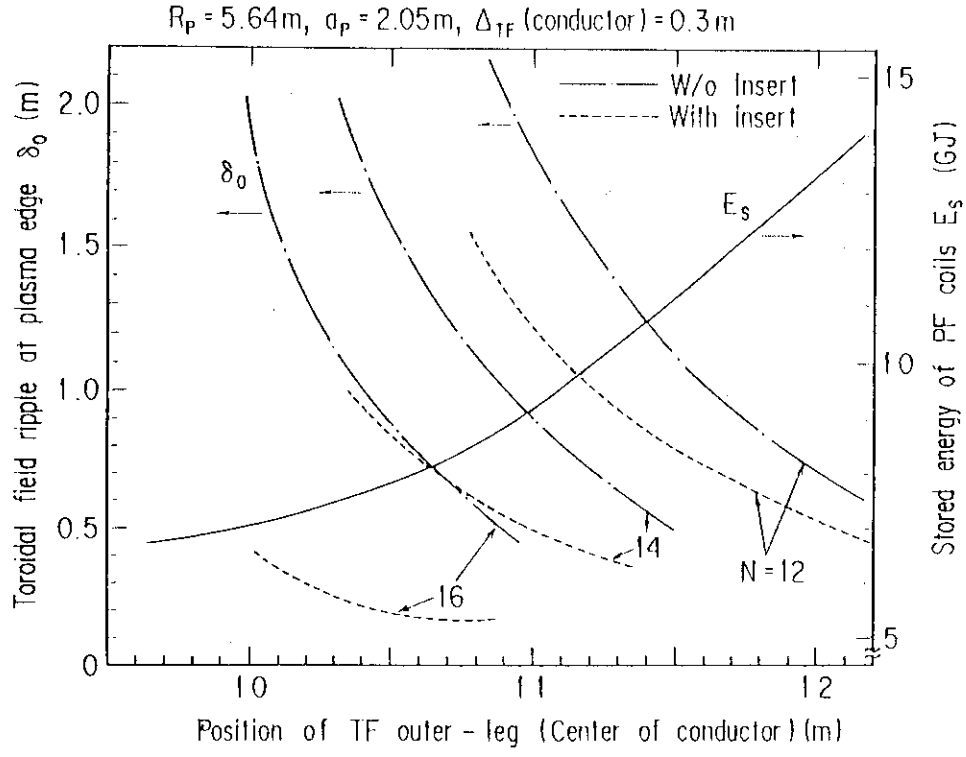

Fig. 1.5-1 Relations between position of TF outer-leg and toroidal field ripple δ_0 at outer plasma edge for three cases of number of toroidal filed coil N (N=12, 14 and 16). Dotted lines show the ripple value when ferromagnetic insert is installed. Solid line shows the total stored circuit energy in Poloidal field system E_s at the end of burn state.

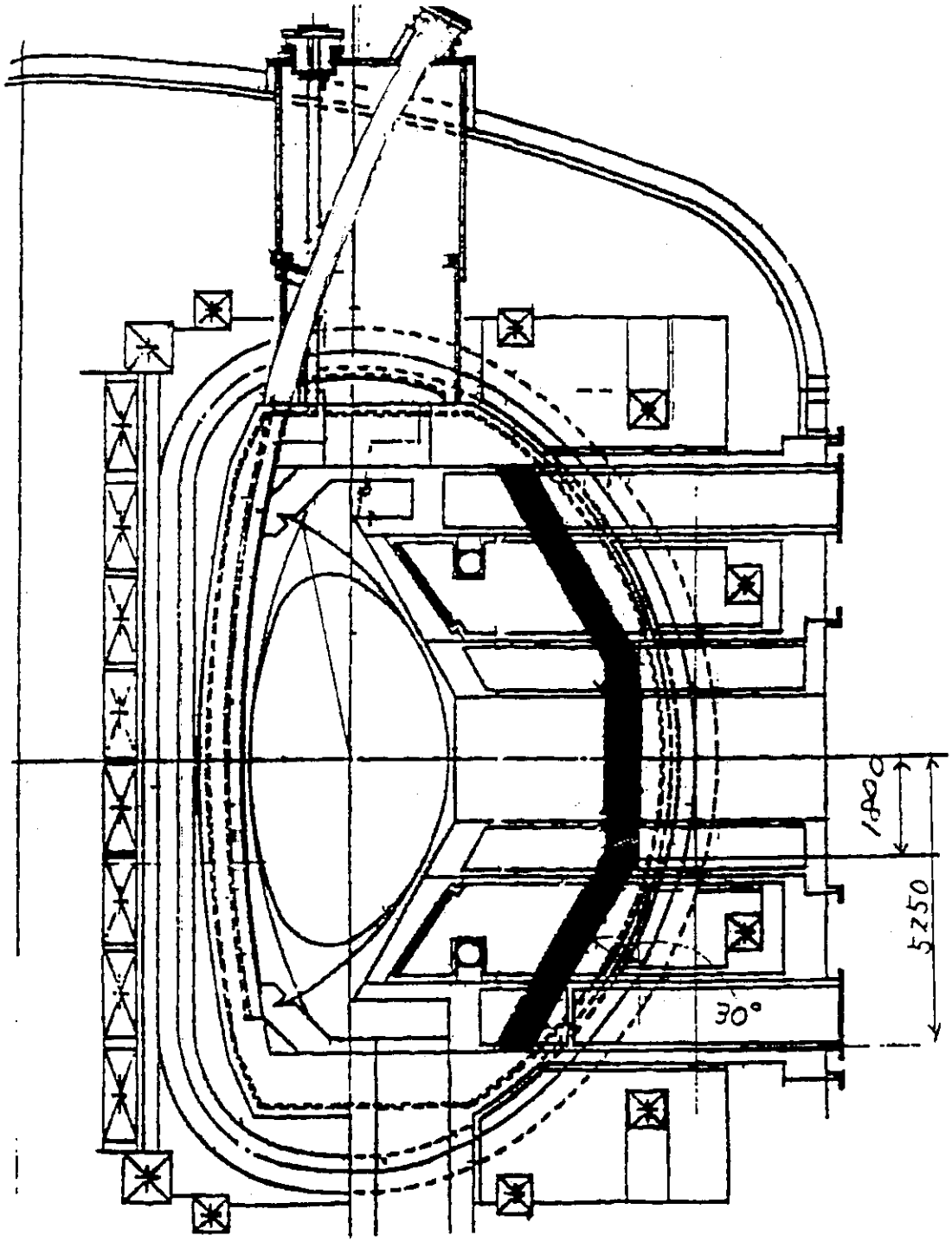

Fig. 1.5-2 Configuration of ferromagnetic insert used in the calculations of Fig. 1.5-1.

2. Flexibility and Extended Operation

In the ITER operation program, H and H-D operations are scheduled in the beginning to confirm various plasma performances and to provide informations and databases for the D-T ignition experiment. Such phased operation is recommended to avoid risks due to uncertainties of the physics database standing on the present tokamak experiments, and requires adequate flexibility for producing various type of plasmas with different shape, size and plasma current. The ITER should be designed to attain such phased operation with adequate flexibility.

In this chapter several optional plasma operations other than the basic plasma will be described, i.e., (1) extended 30 MA plasma operation with increased plasma size, (2) smaller size full blanket plasma operation at technology phase and (3) single null divertor plasma operation with the same major and minor radii as the basic plasma. Coil locations are same as those listed in Table 1.3-1.

2.1 Extended 30 MA operation

Mission of this plasma operation is to recover ignition condition by increasing plasma current and size in case of deteriorated plasma confinement. In order to realize larger plasma size in the extended operation by increasing both major and minor radii, width of the radiation shield structure should be decreased. Plasma parameters are shown in Table 2.1-1 as option E and E1. Only location of the null point is different between two options. The option E1 corresponds to the final state of the moving null point operation for the option E to expand available flux swing at the end of burn. Detail of the moving null point operation will be described in section 3.2.

Ampere-turns distributions of the option E are shown in Fig. 3.2-3 for β_p of 0.1 and 1.0 with different flux linkages. The most distinctive feature of these distributions is large ampere-turns of the PF2 coil, especially for the high β_p plasma. This is due to the increased force to push null point outward against the tendency that the plasma is willing to become natural shape with higher triangularity at high β_p. The linkage flux at the end of burn is limited by the ampere-turns of the PF2 coil in spite of surplus flux supply capability of the PF1 coil. Except the large ampere-turns of the PF2 coil, there are no particular problems in the ampere-turns distribution.

2.2 Technology phase plasma operation

In the technology phase, the plasma is operated with outboard tritium breeding blanket. This requirement results in the decrease of the major and minor radii of the plasma as shown in T1 and T2 of the Table 2.1-1. Option T1 has the same elongation and triangularity as the basic plasma (option B), hence has lower null point location. Option T2, on the contrary, has the same height of the null point location but higher elongation and lower triangularity.

The ampere-turns distribution for both options are shown in Fig. 2.2-1, and the associated stored energy distribution is shown in Fig. 2.2-2. The ampere-turns of the PF5 coil for the option T1 increases by about 30% compared with the basic plasma in spite of the lower plasma current. Stored energy of the PF5 coil therefore reaches 7 GJ at low β_p which exceeds 70% of the total stored energy and is hardly realizable. Such large value is attributed to longer distance between the plasma and the PF5 coil than the basic plasma. One of the possible method to overcomes this difficulty is decreasing triangularity and increasing elongation of the plasma shown as Option T2; both of them mitigate hexapole field requirement of the PF5 coil for the shaping of the plasma cross section. Thus option T2 plasma can be operational within ampere-turns of or with small additive ampere-turns to the basic plasma. Even if the option T1 plasma is operational at high β_p, option T2 plasma should be selected for low β_p by introducing moving null point operation.

2.3 Single null divertor operation

Single null divertor plasma attains smaller total ampere-turns and total stored energy than double null divertor plasma, if the appropriate up-down asymmetry of the elongation and triangularity are selected, which has been already shown in Fig. 1.1-2. In the present study the rate of both elongation and triangularity between active and passive null sides of the plasma is 1.1/0.9. At this rate the total stored energy stays around minimum value.

Figure 2.3-1 depicts ampere-turns distribution of the single null divertor plasma. On the active null side, the distribution retains a feature of the double null divertor plasma, but the ampere-turns are somewhat smaller than those of the double null divertor plasma on the passive null side. The location of the null point is shown in option S of the Table 2.1-1, and is same as the basic plasma. The stored energy distribution is shown in Fig. 2.3-2. Because of large elongation of the active null side of the plasma, usually PF6 coil of this side has maximum stored energy.

This point should be kept in mind in the single null divertor plasma operation.

2.4 Flexibility

In order to maximize operational flexibility, ITER PFC system should be designed to manage all of the options listed in Table 2.1-1. Table 2.4-1 summarizes the macroscopic quantities of all options discussed in the preceding sections. If we exclude the low β_p operation of the option T1 plasma during the technology phase because of quite large stored energy of the shoulder coil (PF5), which can not be recognized as realizable, the maximum total stored energy occurs at low β_p for option E1. Additional stored energy for this operation to the basic plasma operation is 1.7 GJ which is rather small part (~13%) of the total stored energy of the basic plasma in spite of the 50% increase of the plasma current. The 10% additional total ampere-turns can also operate all the options. Therefore, at least from a macroscopic viewpoint, small amount of the additional energy and ampere-turns significantly increases operational flexibility with larger plasma size, increased plasma current by 50% and various plasma shapes including single null divertor plasma configuration.

Figure 2.4-1 depicts overlay of the ampere-turns distributions for all options at both the before heating and end of burn phases. The operation range where all options can be manageable is shown in Fig. 2.4-2 with indicating which phase is critical. Flux linkage at initial magnetization is selected as 95 VS, and that of -160 VS is assumed to be attainable at the end of burn except the technology phase operation. The exact value of attainable flux linkage at the end of burn should be evaluated for each option.

It is strongly recommended that the divertor and outermost coils are designed with 30% and 100% additional current capability of the basic plasma, respectively, in order to operate the extended 30 MA plasma, technology phase plasma with outboard tritium breeding blanket and single null divertor plasma.

Table 2.1-1 Plasma parameter for various options

	B	B1	E	E1	T1	T2	S
I_p (MA)	20	←	30	←	15	←	20
R_p (m)	5.8	←	6.0	←	5.5	←	5.8
a (m)	2.0	←	2.4	←	1.7	←	2.0
Z_p	0	←	←	←	←	←	0.41
κ_{95}	2.0	2.1	1.95	1.88	2.0	2.1	2.0*
δ_{95}	0.35	0.25	0.19	0.28	0.35	0.30	0.35*
R_N (m)	4.75	5.05	5.30	5.00	4.60	4.75	4.75
Z_N (m)	±4.48	±4.70	±5.25	±5.07	±3.80	±4.00	-4.48

* Average value of upper and lower half plasma.
The value is divided into 1.1/0.9 for null/non-null sides.

Table 2.4-1 Macroscopic quantities of various options

(1) β_p = 0.1

	B	B1	E	E1	T1	T2	S
I_p (MA)	20	←	30	←	15	←	20
L_p (MH)	8.40	8.36	8.11	8.07	8.68	8.54	8.35
ψ_p (VS)	-90	←	-100	←	-75	←	-90
E_T (GJ)	13.3	7.74	9.66	15.0	19.5	11.9	6.58
$\Sigma\|I\|$ (MAT)	123	107	106	121	147	120	98.2
$2\pi\Sigma R\|I\|$ (GAT-m)	3.58	2.97	3.28	3.83	4.73	3.36	2.71
ℓ_i	0.79	0.77	0.79	0.80	0.78	0.80	0.76
<n>	-0.91	-0.98	-0.73	-0.66	-1.20	-1.23	-1.08
q^{ψ}(95%)	3.02	3.11	2.49	2.48	3.10	3.35	2.91

(2) β_p = 1.0

	B	B1	E	E1	T1	T2	S
I_p (MA)	20	←	30	←	15	←	
L_p (MH)	9.30	9.23	9.15	9.16	9.39	9.23	9.28
ψ_p (VS)	-150	←	-160	←	-125	←	-150
E_T (GJ)	9.47	8.11	10.5	12.45	11.5	8.21	7.05
$\Sigma\|I\|$ (MAT)	126	130	123	117	137	125	102
$2\pi\Sigma R\|I\|$ (GAT-m)	3.30	3.05	3.51	3.78	3.55	3.09	2.63
ℓ_i	0.83	0.81	0.84	0.84	0.83	0.83	0.81
<n>	-0.71	-0.79	-0.60	-0.52	-0.92	-0.96	-0.74
q^{ψ}(95%)	3.10	3.17	2.55	2.56	3.22	3.41	3.03

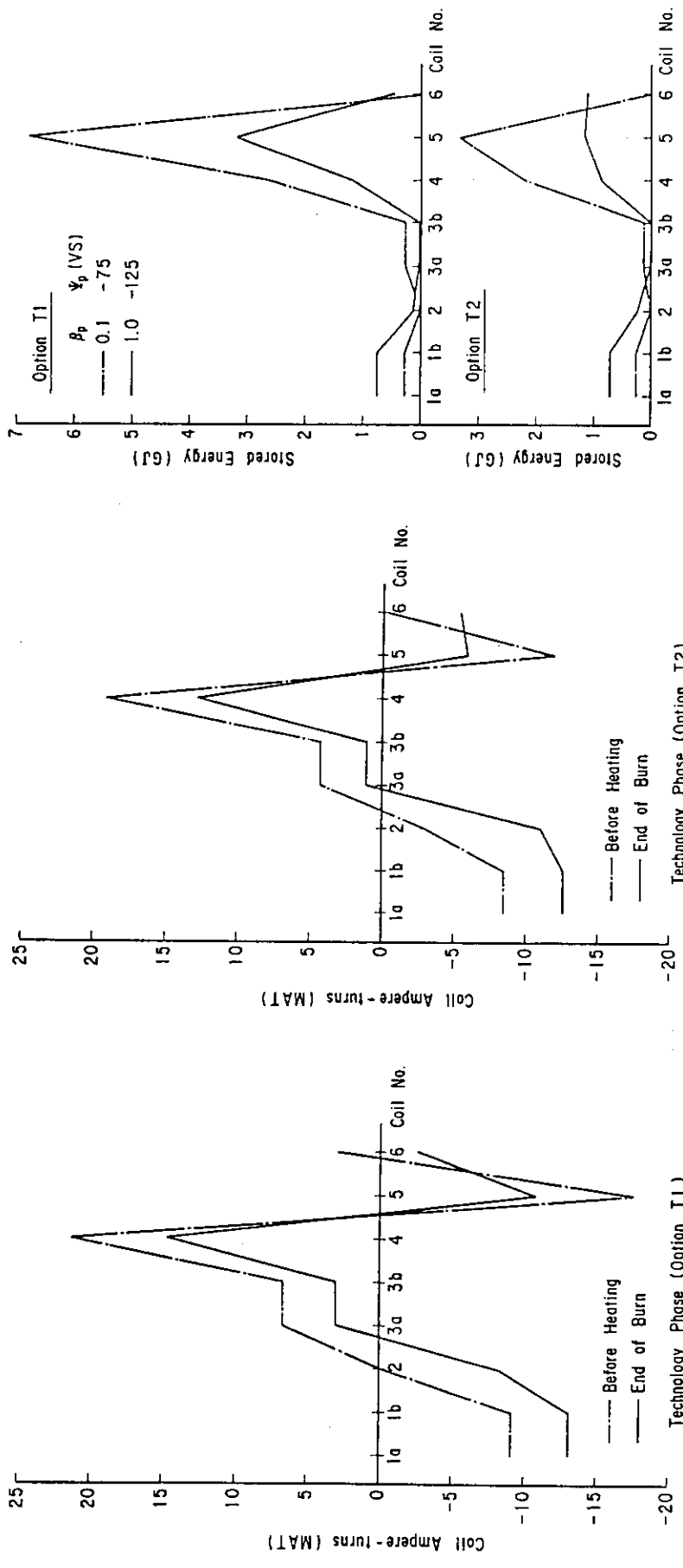

Fig. 2.2-1 Ampere-turns distributions for two cases of the technology phase plasma operation. The option T1 has the same elongation and triangularity as the basic plasma, while option T2 has larger elongation and lower triangularity.

Fig. 2.2-2 Comparison of the stored energy distribution between option T1 and option T2. Quite large value of the stored energy in the shoulder coil for the option T1 at low β_p is not realistic for ITER.

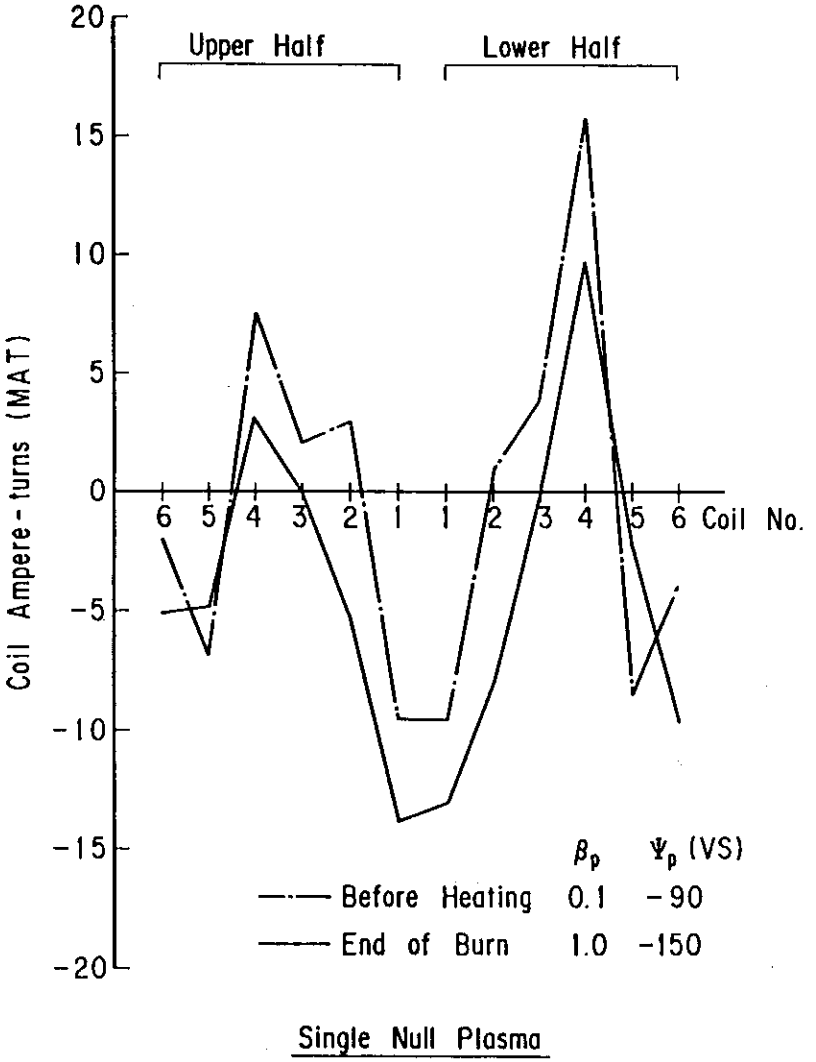

Fig. 2.3-1 Ampere-turns distribution of the single null divertor plasma.

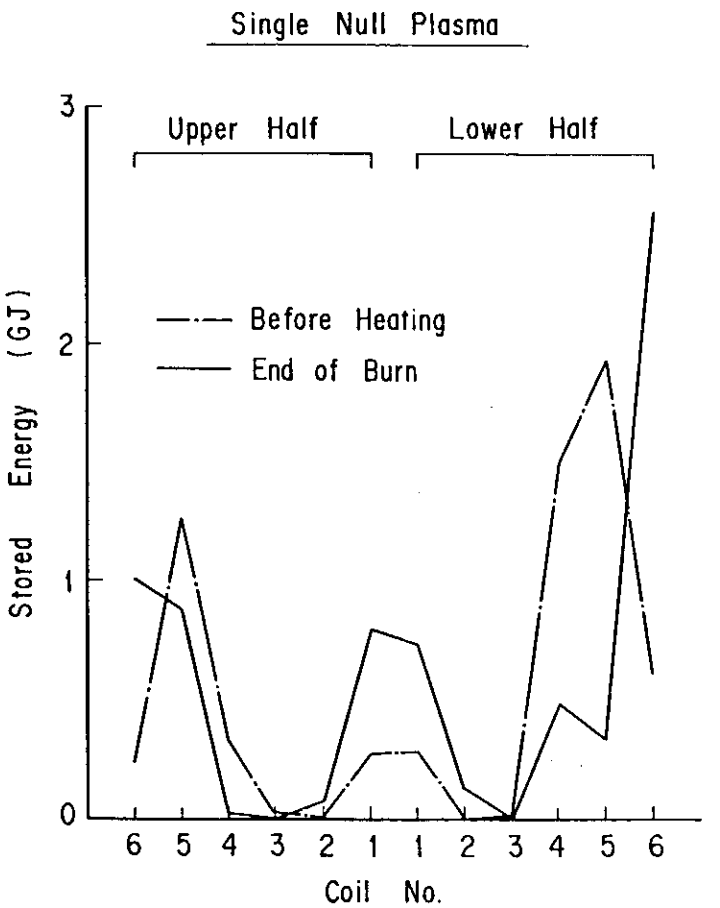

Fig. 2.3-2 Stored energy distribution of the single null divertor plasma.

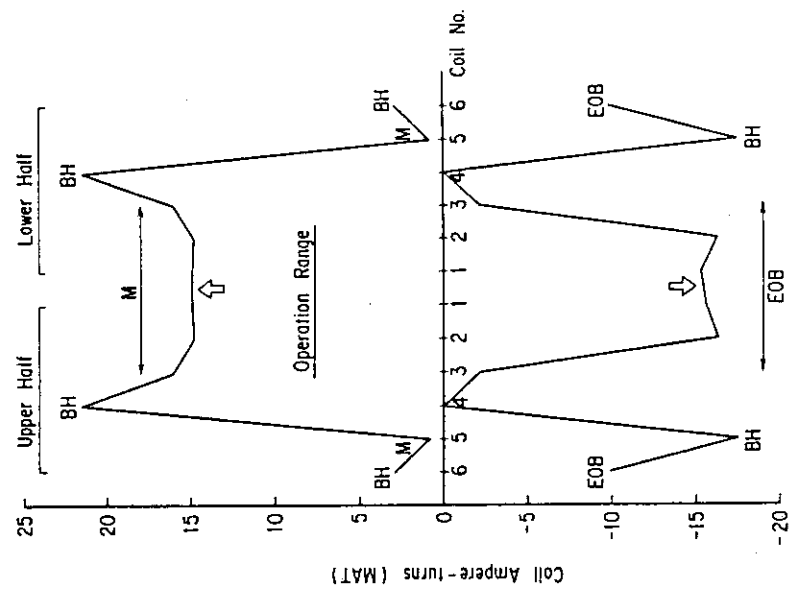

Fig. 2.4-2
Operation range of the PFC for overall plasma options except the low βp operation of the option T1.

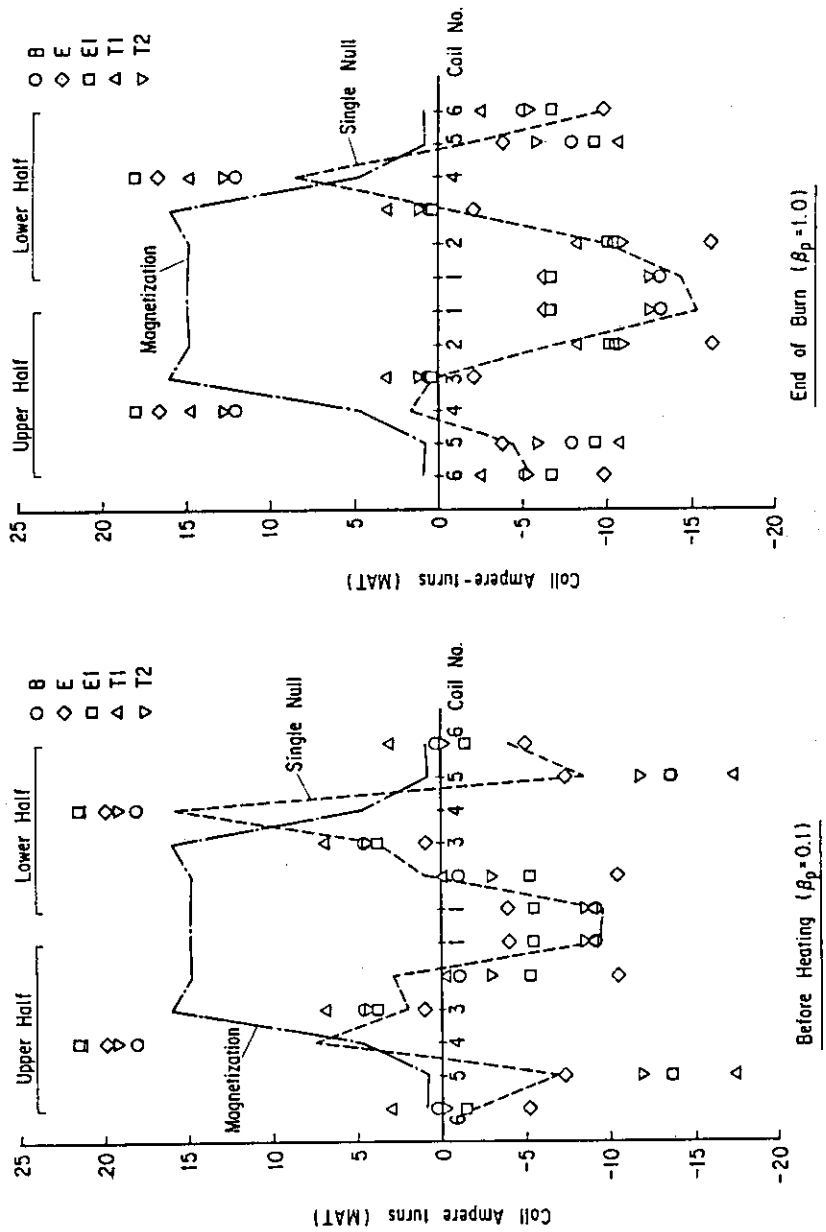

Fig. 2.4-1 Overlay of the ampere-turns distributions for the overall ITER plasma options. Both low and high β_p cases are shown.

3. Equilibrium Control

3.1 Separatrix swing

Separatrix swing is one of the possible ways to mitigate heat load condition of the divertor plate. Separatrix can be swung in any direction if there exists sufficient controllability of the plasma shape in PFC system, while there are some constraints on the AC loss in the super-conducting magnet, available electric power to PFC system, etc.

Because the ampere-turns and the associated stored energy of the PF5 coil are critical from the electric power viewpoint, swing direction was investigated where the ampere-turns change of the PF5 coil during separatrix swing becomes minimum. Figure 3.1-1 displays typical swing directions. The direction for moving null operation, where β_p changes substantially while keeping PF5 ampere-turns almost constant, is also shown in the figure. The constant κ swing (SW1-SW2), which is a most primitive swing method, is not so favorable because 1.2 MAT and 500 MJ changes were observed in the ampere-turns and stored energy of the PF5 coil for the separatrix swing of 30 cm width (Figs. 3.1-2 and 3.1-3), which corresponds to change of δ_{95} by 0.1 around central triangularity of 0.35. If swing frequency of 1 Hz is to be applied, the above stored energy change requires ~1 GW electric power during separatrix swing. Larger changes in ampere-turns were observed on the PF2 and PF3 coils which compensate the change in that of the PF5 coil, but change in the stored energy are almost equal (PF4) or smaller (PF2) because of smaller self-inductance of these coils.

As an ampere-turns corresponding to the hexapole magnetic field is assumed to occupy a large part in the PF5 coil, constant hexapole field swing (SW3-SW4) seems to minimize ampere-turns change of PF6 coil. Hexapole magnetic field normalized by $\mu_0 I_p/2\pi a$ to produce a plasma with an elongation, triangularity and poloidal beta of κ, δ and β_p, respectively, has a proportionality as

$$b_H \propto C_1\delta/\kappa^2 - C_2\beta_p \qquad (C_1, C_2>0) \qquad (1).$$

A constant δ/κ^2 swing is a candidate for the above purpose. The direction of the swing is shown in Fig. 3.1-1, and is almost rectangular to the direction of moving null point operation. Ampere-turns change of the PF5 coil is rather larger than that of constant κ swing resulting in huge change in the stored energy of about 1.1 GJ. This phenomenon suggests that fairly large part of the ampere-turns comes from quadrapole magnetic field.

Intermediate swing direction shown as SW5-SW6 in Fig. 3.1-1 showed good result in changes in ampere-turns and stored energy of PF5 coil. Only divertor coil (PF4) is still associated with large change in stored energy. Further optimization will be possible by sharing changes in ampere-turns and stored energy in all coils by small amount. On the other hand minimum swing amplitude and frequency should be investigated by carefully examining divertor heat load and cooling condition. Combination of in-TFC swing coil should also be investigated in detail.

Table 3.1-1 summarizes macroscopic quantities for various separatrix swings. For these values there is no problems in separatrix swing.

3.2 Moving null point operation

For PFC configuration with shoulder coil (PF5) far apart from plasma like ITER reference design, ampere-turns and its associated stored energy tend to become quite large, especially at low β_p, if a high triangularity plasma should be attained. Usually maximum of the total stored energy appears at the time of maximum plasma current and low β_p, e.g., before heating for the ITER reference PFC configuration. In order to realize effective use of the PFC system, maximum of the total stored energy is required to appear at the end of burn.

The idea of the moving null point operation was introduced in this section to overcome above difficulty. This idea bases on the fact that main part of the shoulder coil ampere-turns comes from producing hexapole magnetic field, and that the hexapole magnetic field normalized by $\mu_0 I_p/2\pi a$ scales as Eq. (1). This relationship suggests that the stored energy of the shoulder coil can be reduced (in absolute sense) by lowering δ/κ^2 at low β_p. Combination of reducing δ and increasing κ is most effective for this purpose, and fortunately the direction of the null point motion is almost parallel to the divertor plate as shown in Fig. 3.2-1. Moving null point operation will be described for both the basic and extended plasma hereafter.

Figure 3.2-2 compares ampere-turns distributions for the basic plasma between fixed and moving null point operations. In the moving null point operation, ampere-turns of the shoulder and divertor coils at low β_p decrease, and the stored energies of these coils therefore decrease as shown in Fig. 3.2-4. In addition, the change in the stored energy of the outermost coil also decreases resulting in reduction of the electric power requirement. Similar results are shown in Figs. 3.2-3 and 3.2-5 for the extended plasma, but as far as reduction of the stored energy is concerned it is not remarkable.

Deterioration of vertical stability at low β_p may happen in the moving null point operation, because both lower triangularity and higher elongation cause the decay index more negative. This point must be examined in detail in the moving null point operation.

3.3 Possible range of l_i

The degree of plasma current peaking, which is approximately represented by internal inductance l_i, affects flux consumption and also ampere-turns distribution in some extent, though the effect is not so decisive as plasma shape and β_p. As the flux swing requirement is one of the determinative factor of a reactor size, it is important to evaluate range of l_i beforehand.

In the equilibrium calculation for this purpose, the following type of the plasma current profile was employed and three cases of n values, i.e., 0.5, 1.0 and 2.0, were investigated while the values of m were automatically decided so that safety factor on the magnetic axis, q(0), become unity.

$$j_p(\tilde{\Psi}) \propto \left\{ R + \frac{R_p^2}{R}\left(\frac{1}{\beta_J} - 1\right)\right\}\left\{1 - \left(1 - \tilde{\Psi}\right)^n\right\}^m$$

where $\tilde{\Psi}=(\Psi-\Psi_S)/(\Psi_M-\Psi_S)$ and β_J is an approximate value of β_p.

Figure. 3.3-1 shows the dependence of l_i on the safety factor at the flux surface in which 95% of the flux between the magnetic axis and plasma surface is included. Equilibria were calculated with plasma currents of 10, 12.5, 15, 20 and 30 MA for both the low and high poloidal betas of 0.1 and 1.0. At 30 MA plasma current, β_p=1 equilibrium could not be obtained for q(0)=1 with the above group of the plasma current profile, because even the flat profile (m=0) has lower q(0) than unity.

The figure shows almost linear dependence between l_i and $q(\tilde{\Psi}=0.95)$ - q(0). For the same value of n, high β_p plasmas have slightly lower l_i values in a manner of parallel displacement from low β_p plasma. Though l_i exceeds 1.5 for high value of n and low plasma current, e.g. n=2 and Ip=10 MA, the safety factor on the magnetic axis does not seem to fall down to unity for such low plasma current in the normal operation. Figure 3.2-2 depicts plasma current profile for three different values of n, i.e., 0.5, 1.0 and 2.0. If a class of equilibrium with almost parabolic current profile by setting m=1.5 and n=1.0 is investigated, q(0) has a value of about 2 at 10 MA plasma current and l_i stays around 0.8 for wide range of I_p and β_p. For the equilibrium calculation to estimate PFC system values, it is recommended to employ the

value of l_i ranging from 0.6 to 1.2; the upper bound corresponds to about 1.5 times of the l_i for almost parabolic plasma current.

3.4 Horizontal movement due to thermal quench

During disruption current quench of the order of millisecond is usually preceded by faster thermal quench, whose time scale is roughly 100 μs, resulting in rapid decrease of poloidal beta and imbalance of the equilibrating force. The poloidal field coils can not follow such quick change, so the plasma will move inward while conserving its linkage flux. Flux inside the vacuum vessel is also assumed to conserve for such fast plasma motion due to eddy current generation.

Displacement and deformation of the plasma during thermal quench at disruption was studied as follows keeping the above discussion in mind;

(1) Initial plasma equilibrium was calculated for the prescribed plasma shape, position and poloidal beta. Boundary meshes of the calculation were located approximately at the vacuum vessel position.

(2) By using poloidal flux distribution at the boundary meshes for the initial equilibrium, a series of new plasma equilibria were calculated for smaller values of poloidal beta without imposing any condition on plasma shape and position. Total plasma current was kept constant during these equilibrium calculations.

Figure 3.4-2 shows change of plasma equilibrium during thermal quench. At β_p=0.01 ($\Delta\beta_p$=0.99), plasma surface is limited by the guard limiter which locates 15 cm apart from the separatrix of the initial divertor plasma. Flux conservation of the plasma is guaranteed in Fig. 3.4-3 as an almost constant profile of $\Psi_p+L_pI_p$, while the external linkage flux, Ψ_E, decreases along with shrinkage of the major radius. Changes of the major radius, R_p, and the position of the inside plasma surface, R_p-a, are shown in Fig. 3.4-4. Major radius decreases by about 30 cm during thermal quench, but the displacement of the inside plasma surface amounts only 15 cm. On the other hand, the null point almost remains at the height of the initial position as shown in Fig. 3.4-5. These results show that the elongation of the plasma increases during thermal quench which might enhance the positional instability in the vertical direction.

Although the above investigation is still primitive, it should be concluded that plasma fairly moves inward due to thermal quench.

Table 3.1-1 Macroscopic quantities for various separatrix swings.

	B	SW1	SW2	SW3	SW4	SW5	SW6
R_N (m)	4.75	4.60	4.90	4.69	4.81	4.62	4.87
Z_N (m)	4.48	←	←	4.59	4.37	4.50	4.43
I_p (MA)	20	←	←	←	←	←	←
L_p (MH)	9.30	9.24	9.36	9.15	9.40	9.20	9.38
ψ_p (VS)	-150	←	←	←	←	←	←
E_T (GJ)	9.47	9.17	9.77	8.10	11.2	8.81	10.2
$\Sigma\|I\|$ (MAT)	126	121	131	117	136	121	133
$2\pi\Sigma R\|I\|$ (GAT-m)	3.30	3.21	3.38	3.03	3.58	3.16	3.45
ℓ_i	0.83	0.84	0.83	0.85	0.85	0.86	0.84
<n>	-0.71	-0.68	-0.75	-0.72	-0.73	-0.70	-0.75
q^{ψ}(95%)	3.10	3.20	2.99	3.31	2.95	3.24	2.98

Above values correspond to the time of end of burn.

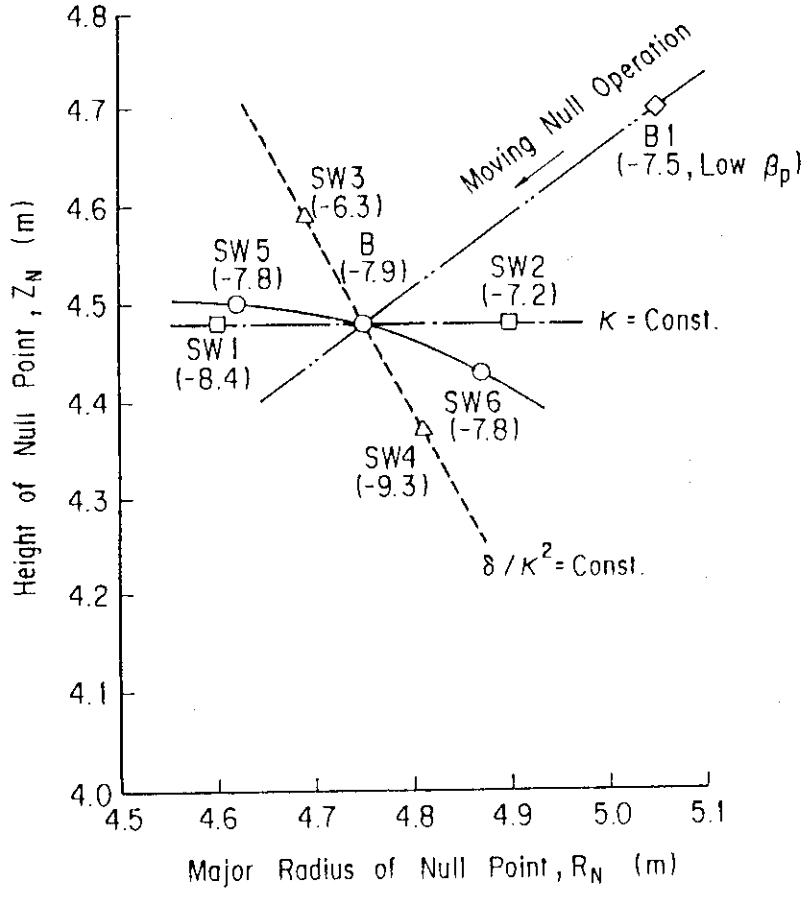

Fig. 3.1-1 Loci of the null point for various separatrix swings of the basic plasma. The direction of the moving null point operation is also shown.

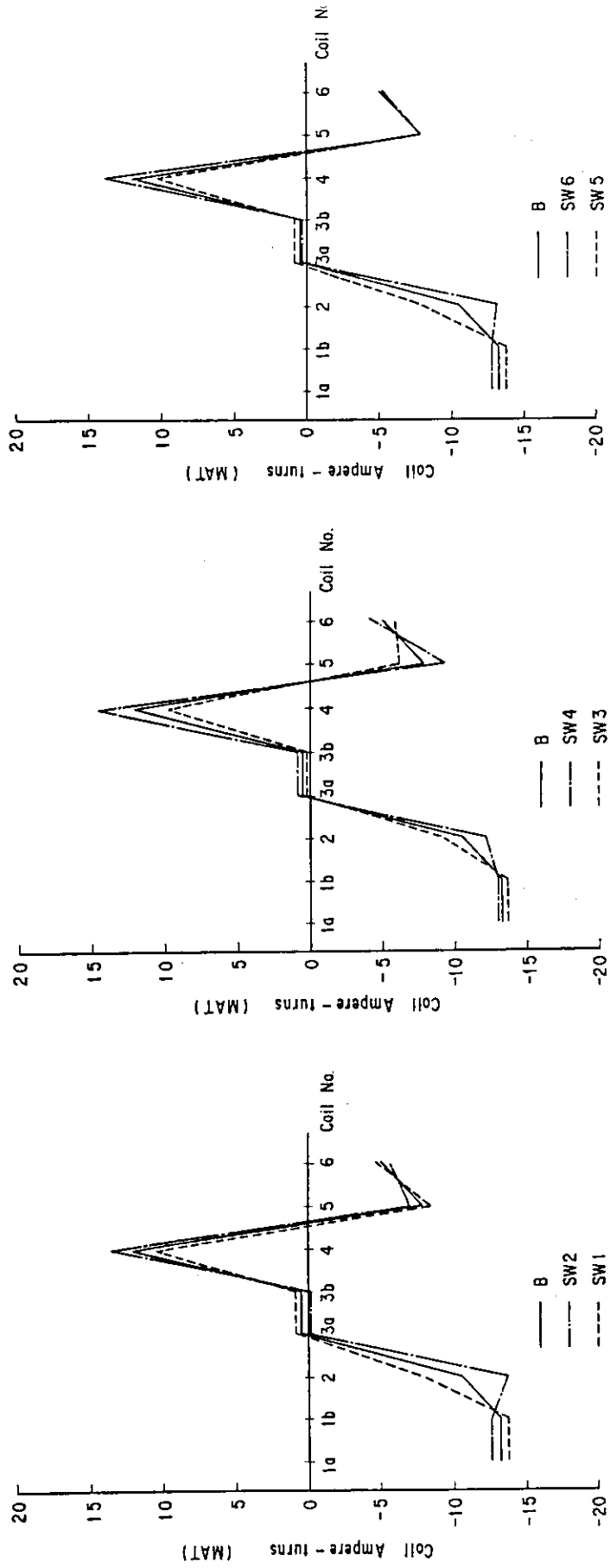

Fig. 3.1-2 Changes in the ampere-turns distribution for (a) constant κ, (b) constant δ/κ^2 and (c) intermediate separatrix swing.

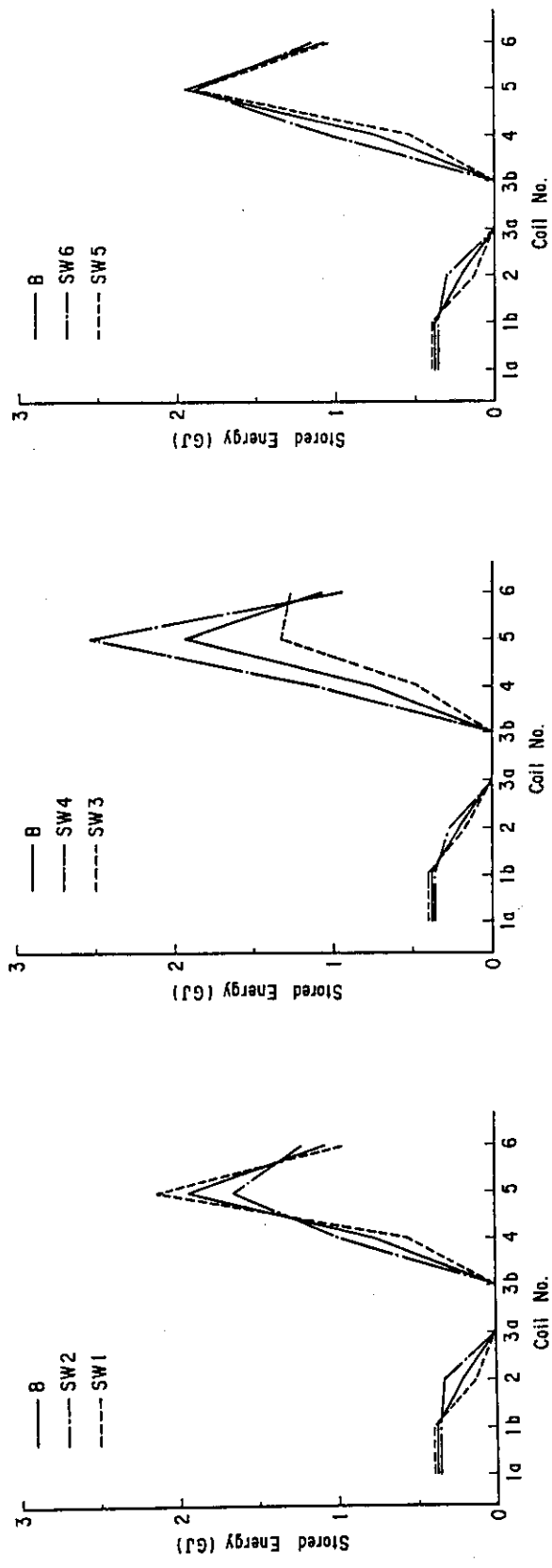

Fig. 3.1-3 Changes in the stored energy distribution for (a) constant κ, (b) constant δ/κ^2 and (c) intermediate separatrix swing.

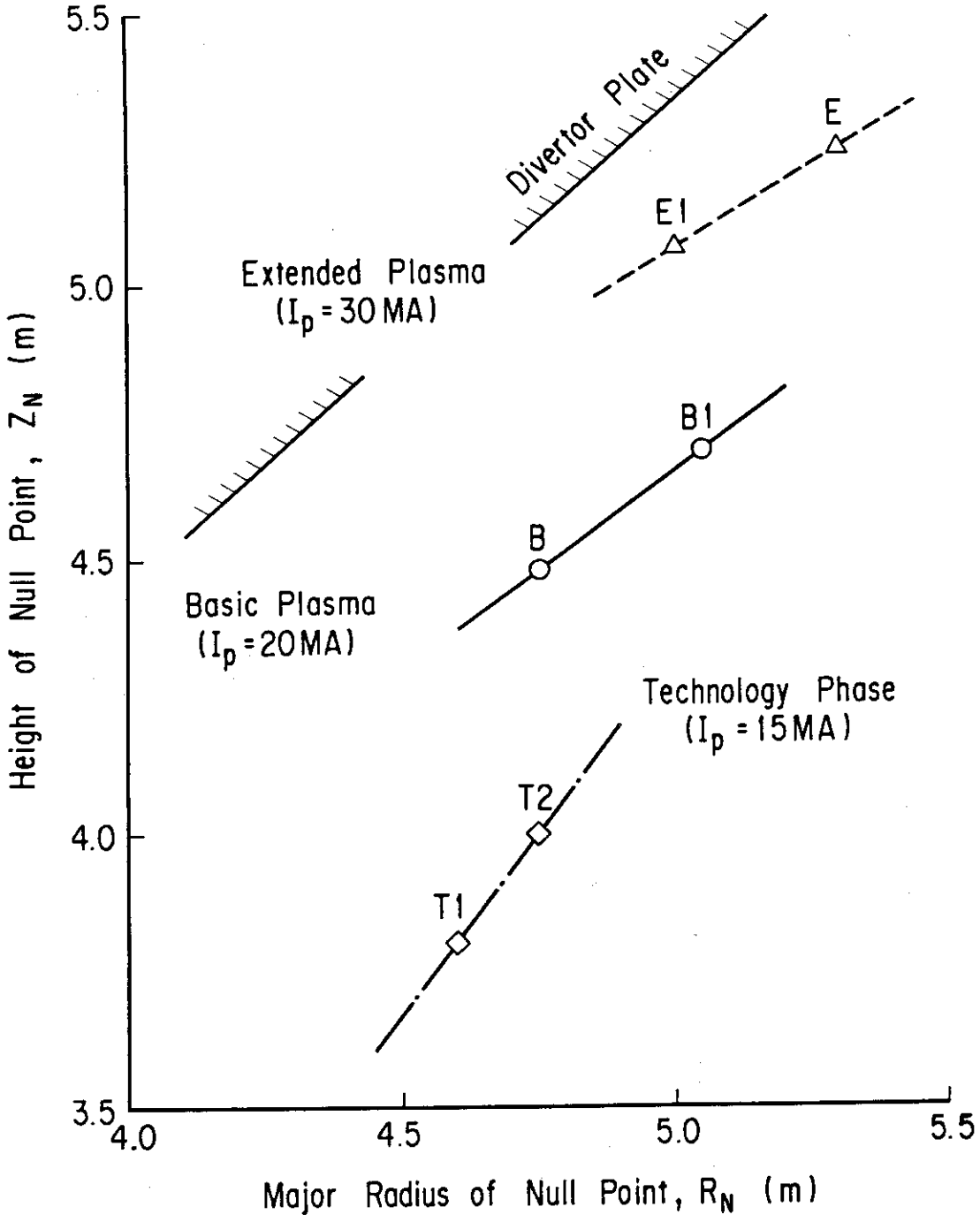

Fig. 3.2-1 Loci of the null point during moving null point operation for the basic plasma (B1→B), extended plasma (E→E1) and technology phase plasma (T2→T1).

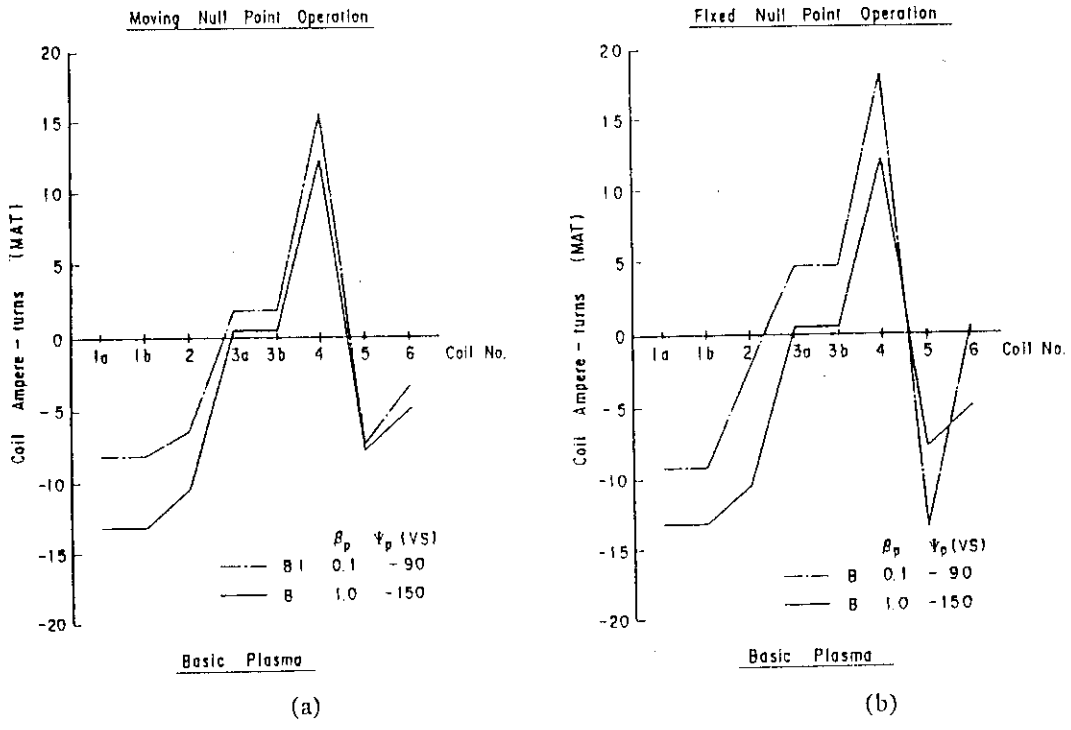

Fig. 3.2-2 Comparison of the changes in the coil ampere-turns between (a) moving null point operation and (b) fixed null point operation for the basic plasma.

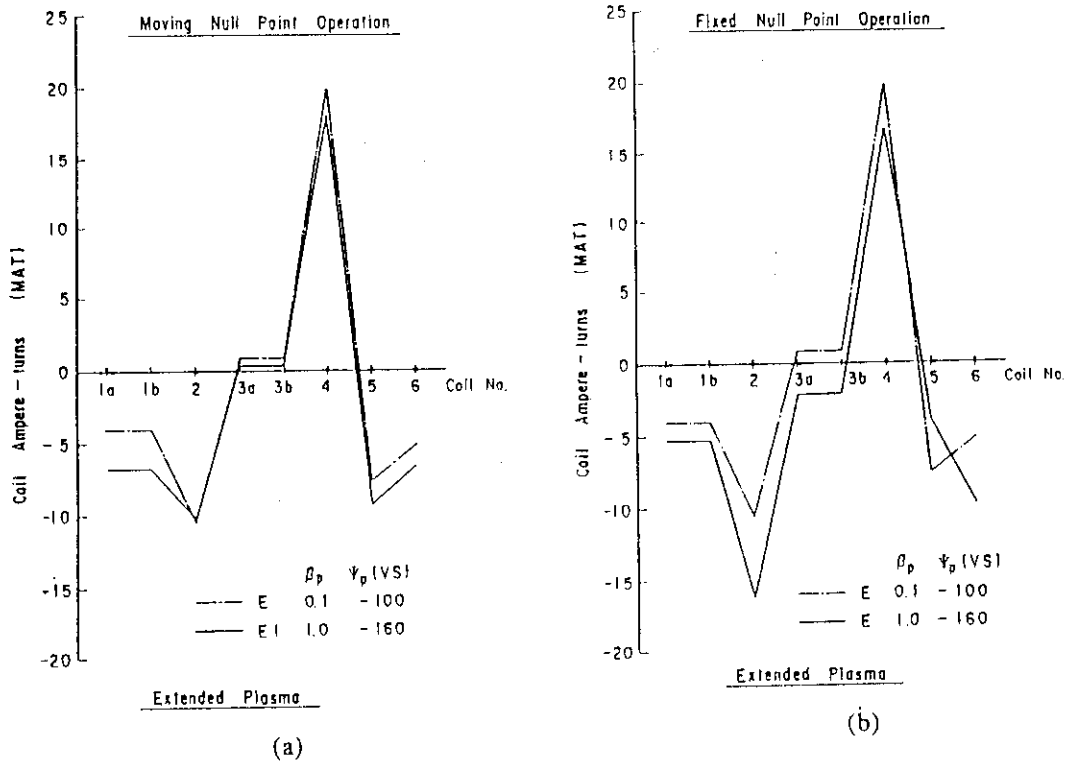

Fig Fig. 3.2-3 Comparison of the changes in the coil ampere-turns between (a) moving null point operation and (b) fixed null point operation for the extended plasma.

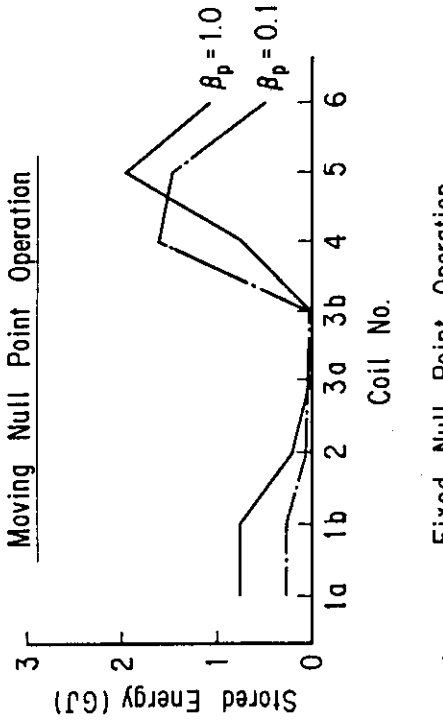

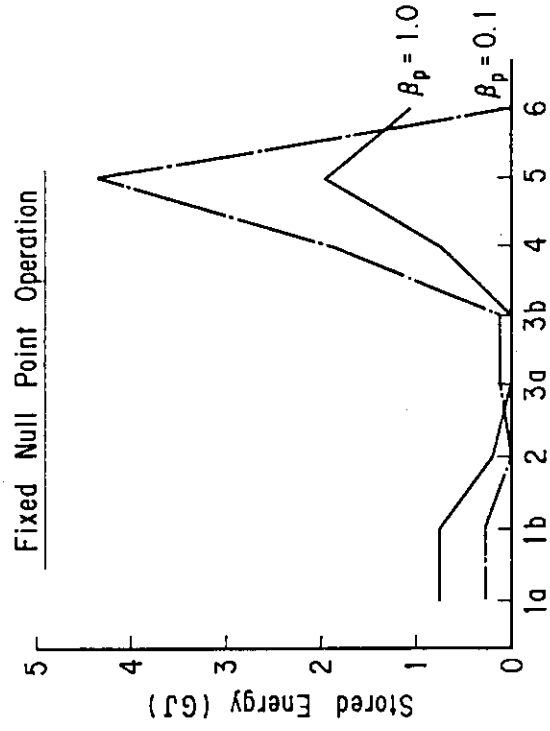

Fig. 3.2-4 Comparison of the changes in the stored energy between (a) moving null point operation and (b) fixed null point operation for the basic plasma.

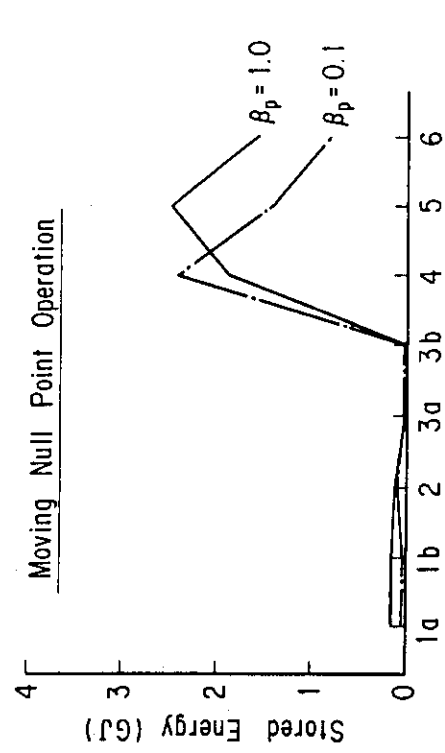

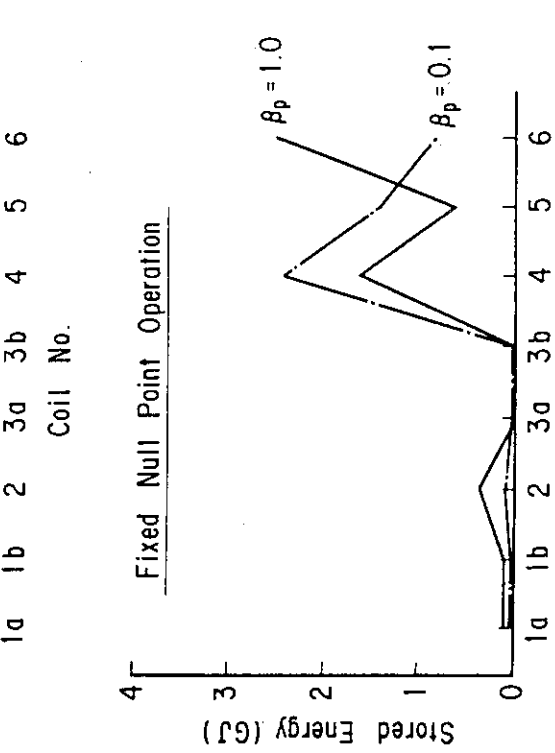

Fig. 3.2-5 Comparison of the changes in the stored energy between (a) moving null point operation and (b) fixed null point operation for the extended plasma.

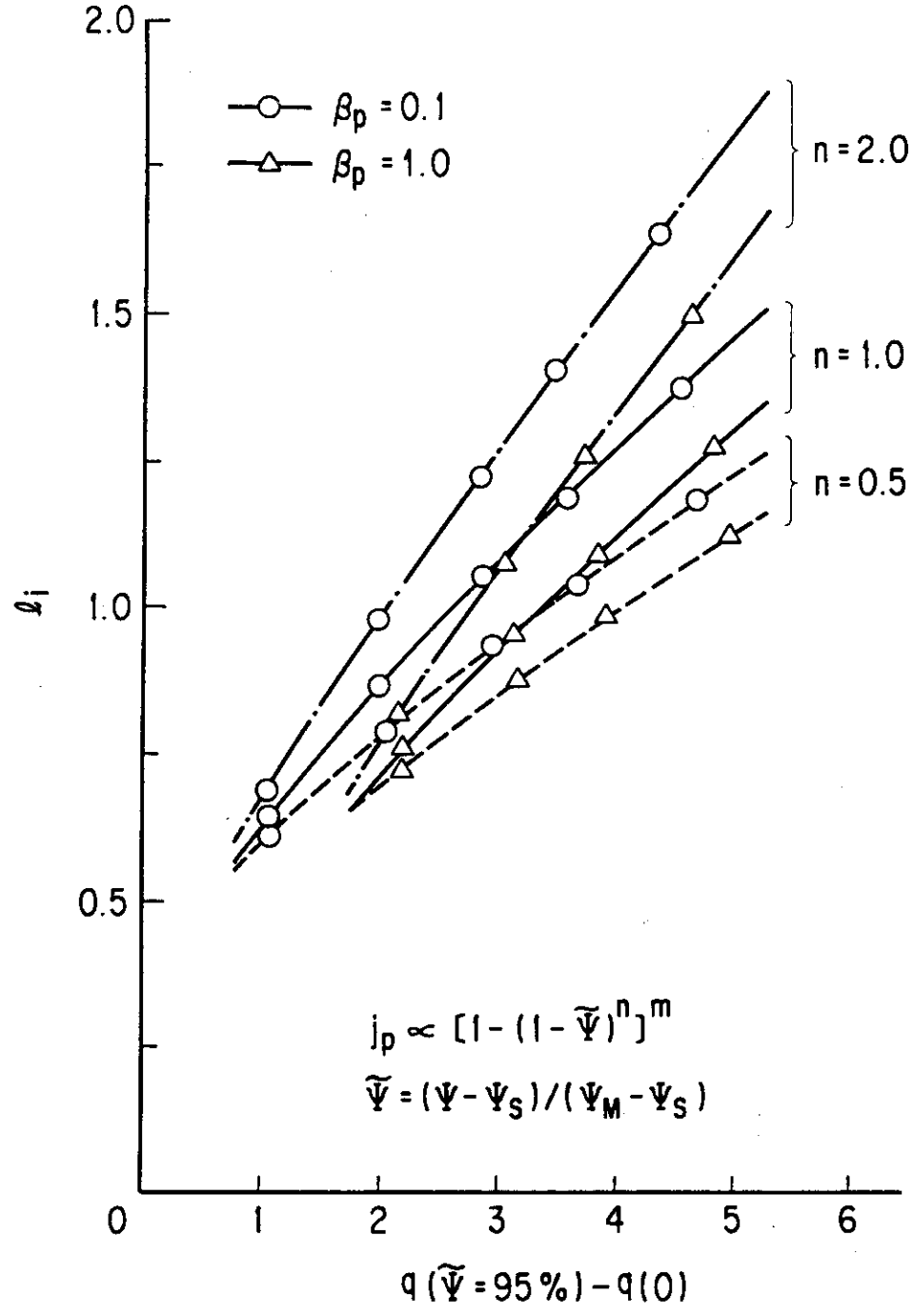

Fig. 3.3-1 Safety factor dependence of the internal inductance, li, for different set of plasma current density profiles: (a) n=0.5, (b) n=1.0 and (c) n=2.0. Safety factor on the magnetic axis, q(0), is fixed at unity.

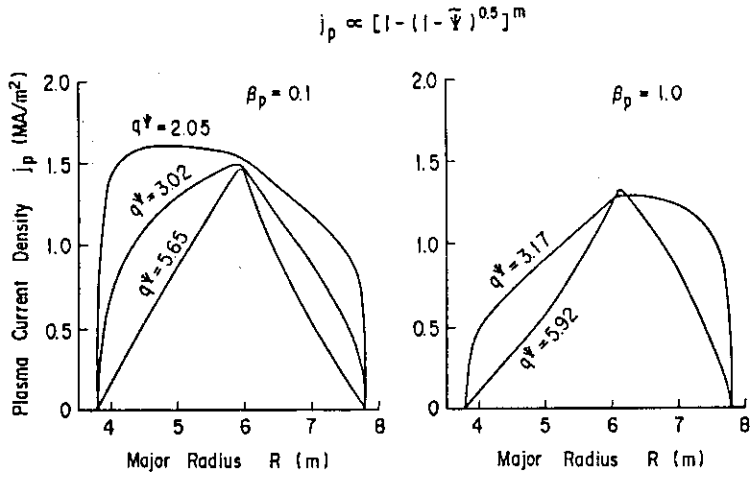

(a)

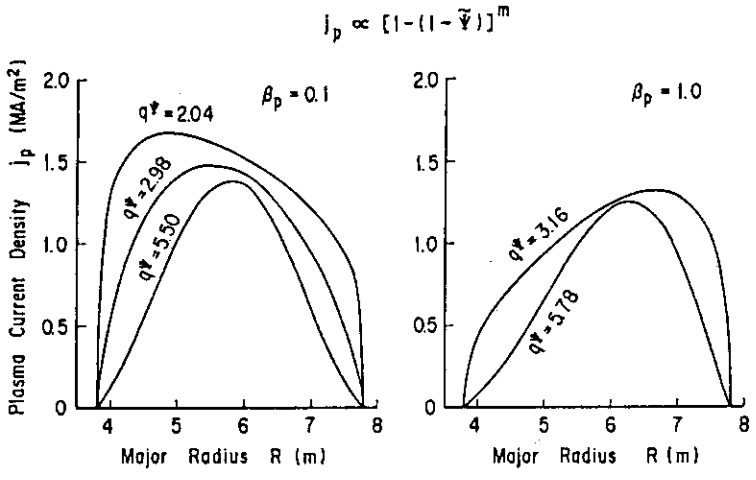

(b)

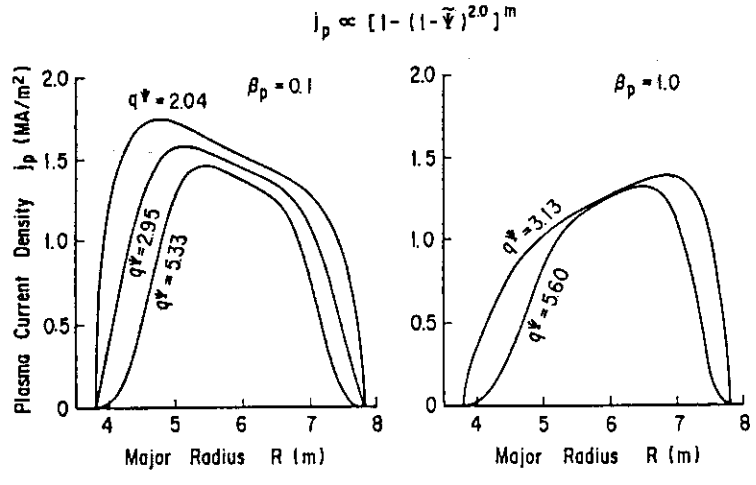

(c)

Fig. 3.3-2 Plasma current density profiles with different safety factor at the 95% flux surface, q^Ψ, i.e., different total plasma current. The values of n are the same as the result shown in Fig. 3.3-1.

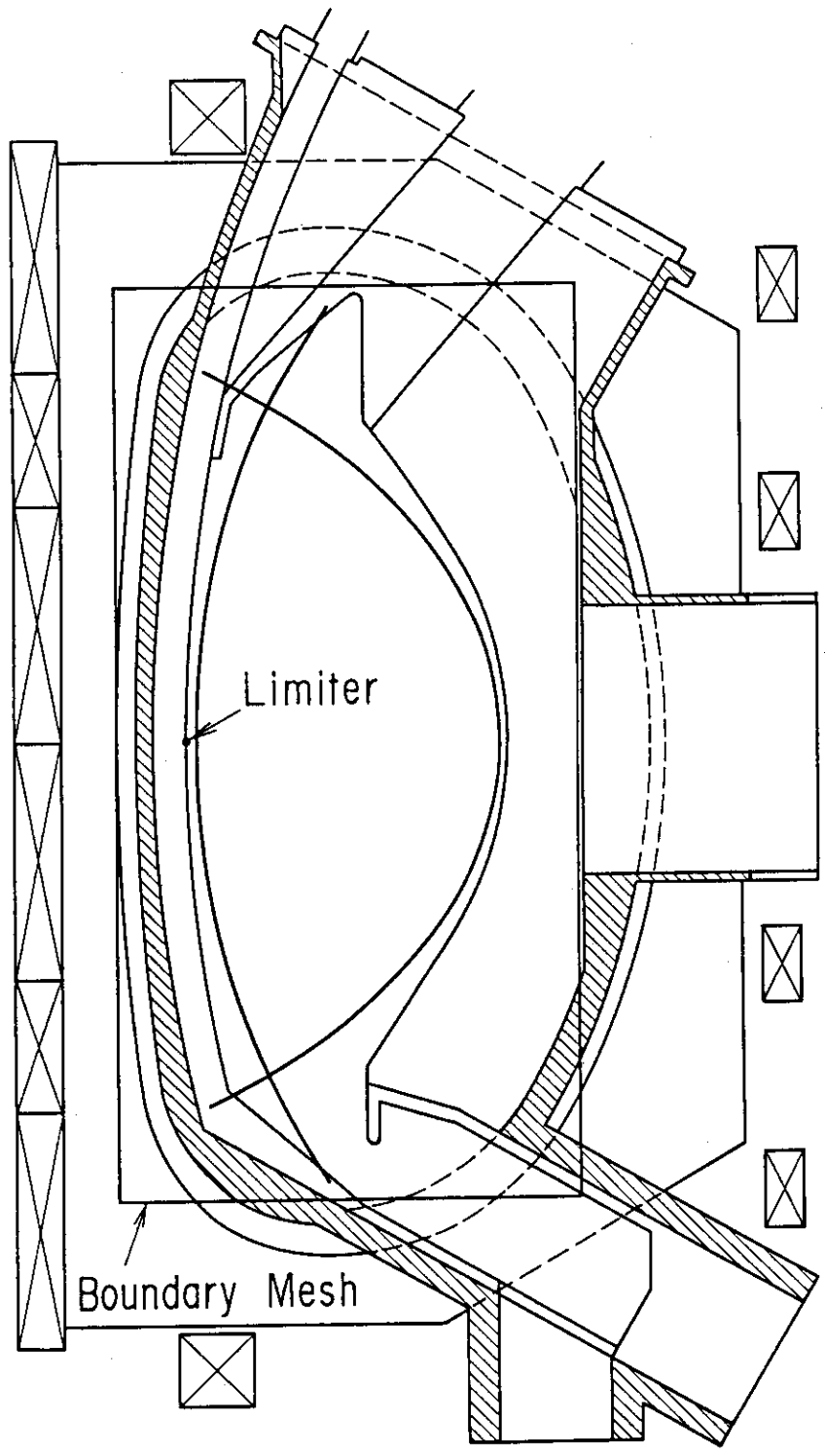

Fig. 3.4-1 Location of the boundary meshes for calculating plasma movement during thermal quench at disruption. Flux values on the boundary meshes were kept constant to simulate flux conservation.

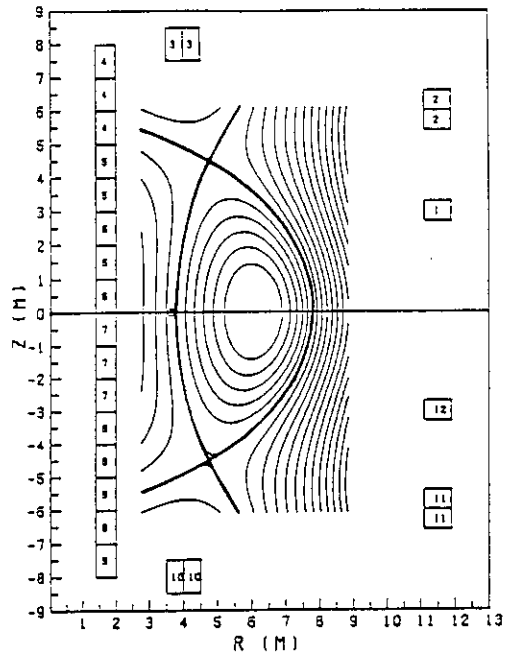

(a) β_p = 1.0

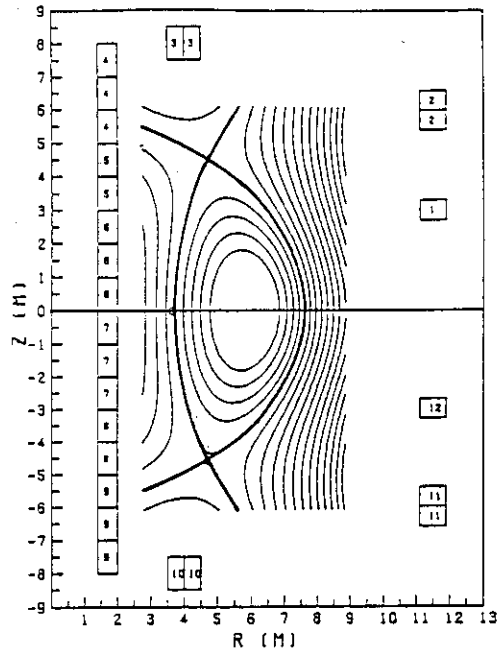

(b) β_p = 0.5

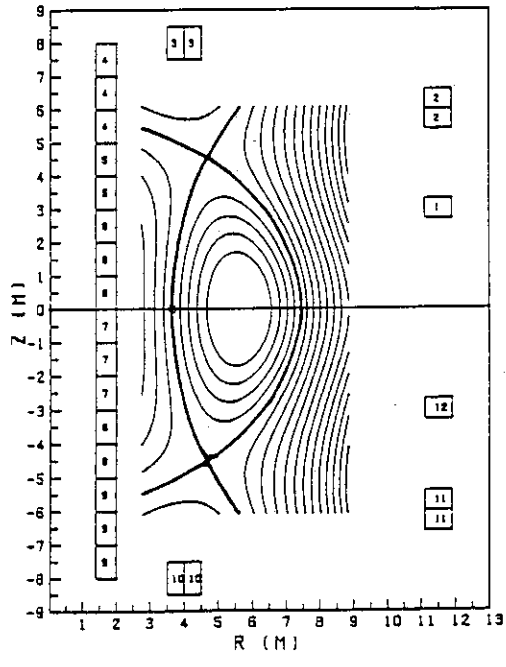

(c) β_p = 0.1

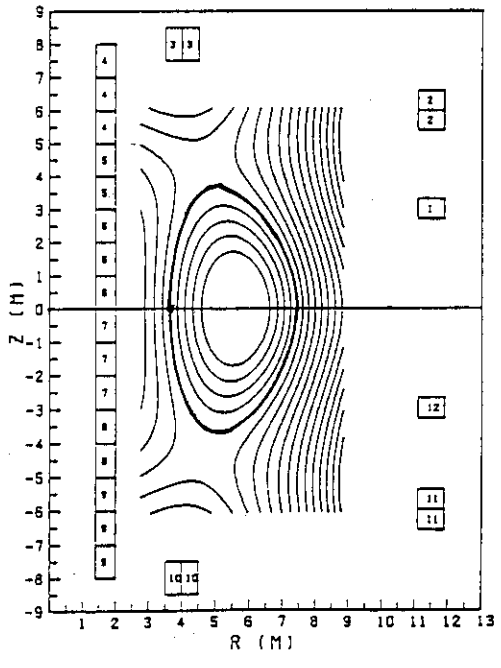

(d) β_p = 0.01

Fig. 3.4-2 Change of the plasma shape and position during thermal quench; (a) initial plasma with β_p=1.0, (b) β_p=0.5, (c) β_p=0.1 and (d) β_p=0.01. At β_p=0.01, inside plasma surface touches the limiter located 15cm apart from the surface of the initial plasma.

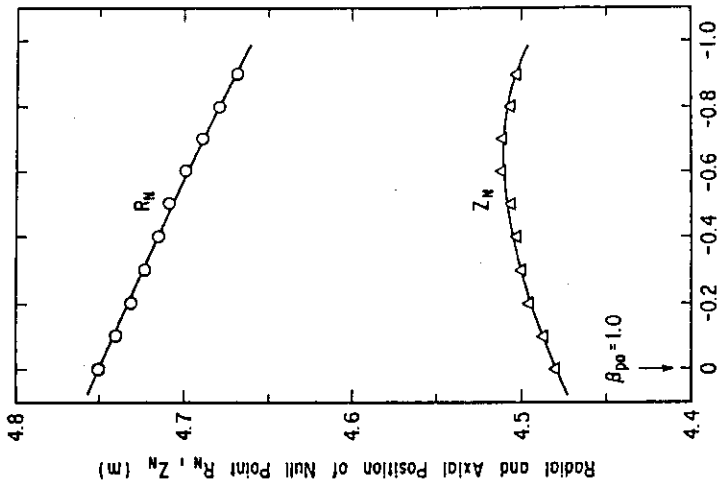

Fig. 3.4-5
Change of the null point location.

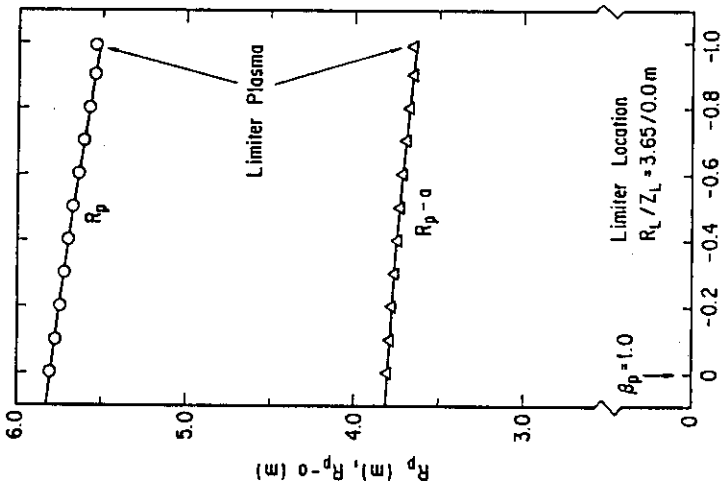

Fig. 3.4-4
Changes of the major radius and the location of the inside surface of the plasma.

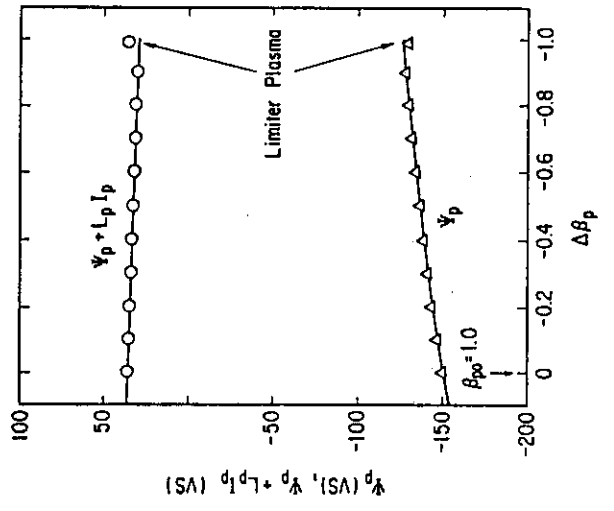

Fig. 3.4-3
Certification of the flux conservation by the plasma. $\Psi_p+L_pI_p$ corresponds to the total flux linkage to be conserved.

4. Related System Quantities Based on Equilibrium Calculation

4.1 Fusion power output

In this section, exact fusion power output from the ITER basic plasma is evaluated based on the equilibrium analysis. Correction factor for the calculation with average density and temperature of fuel ions is also evaluated by comparing with the exact fusion power output calculation. The total beta value is 3.6% and 2.8% is assumed to be contribution from both fuel ions and electrons released from fuel ions. This value corresponds to the average fuel density of 0.92×10^{20} m^{-3} and temperature of 10 keV. Equal mixing ratio of the deuterium and tritium is assumed, so the average deuterium or tritium density is 0.46×10^{20} m^{-3}.

Two pressure profiles are employed in the equilibrium calculation, i.e., $p \propto \tilde{\Psi}^{1.5}$ and $\tilde{\Psi}^{1.3}$, where $\tilde{\Psi}$ is poloidal flux normalized by flux difference between the magnetic axis and plasma surface. For both pressure profiles the temperature profile is assumed to be $\tilde{\Psi}$, so the density profile is reduced to be $\tilde{\Psi}^{0.5}$ or $\tilde{\Psi}^{0.3}$. These profiles simulate recent experimental results in which relatively peaked temperature but flat density profiles are attained in the large tokamaks.

Only D-T fusion reaction is considered and the following temperature dependence of the reaction rate, $\langle \sigma v \rangle$, is employed.

$$\langle \sigma v \rangle = 1.0 \times 10^{-22} \exp[a_1 X^3 + a_2 X^2 + a_3 X + a_4] \quad (m^3/s)$$

where $X = \ln T$, $a_1 = 0.038245$, $a_2 = -1.0079$, $a_3 = 6.3977$ and $a_4 = -9.75$, and T is measured in KeV. Using above expression of $\langle \sigma v \rangle$, fusion power output is calculated by the following relation.

$$P_f = \int \frac{1}{4} n \left(\tilde{\Psi}\right)^2 \langle \sigma v \rangle E_f \, dV$$

where E_f is energy released by a D-T reaction.

Figure 4.1-1 shows average temperature dependence of fusion power output. The average fuel density was changed so that the fuel pressure is kept constant. Flattening of the density profile from $\tilde{\Psi}^{0.5}$ to $\tilde{\Psi}^{0.3}$ results in decrease of the fusion power output by about 5% due to decrease of the fuel particles at high temperature region where fusion reaction rate is large.

As the average fuel pressure is kept constant, $\bar{n}$ scales as $\bar{T}^{-1}$ resulting in fusion reaction power scaling as $\bar{n}^2 \langle \sigma v \rangle \propto \bar{T}^{-2} \langle \sigma v \rangle$. In the considered temperature range, $\langle \sigma v \rangle$ increase slower than T^2, so

the fusion power output decreases as the average temperature increases.

Correction factor for the fusion power output evaluated with average quantities is defined as follows;

$$C_f = \int \frac{1}{4} n\left(\tilde{\Psi}\right)^2 \langle \sigma v \rangle E_f \, dV \; / \; \frac{1}{4} \bar{n}^2 \langle \sigma v(\bar{T}) \rangle \int dV$$

Figure 4.1-2 shows the average ion temperature dependence of the correction factor. Basically Fig. 4.1-2 reflects dependence of the fusion power output on the average ion temperature. Calculations for the total beta of 6% were also carried out to see the geometrical effect of the nested magnetic surfaces. Beta value of the fuels was fixed as the same, i.e., 2.8%. No sensible change is observed. This is due to relatively small poloidal beta value even for the high total beta value ($\beta_p \approx 1$ at β=6%).

In the ITER design, the average temperature of 10 KeV is selected, so the correction factor of 1.5-1.7 should be employed in the fusion power output estimation.

4.2 Magnetic quantities in scrape-off region

Divertor plasma simulation to study helium ash exhaust, remote radiative cooling, etc., requires informations about the connection length between the median plane and divertor plate, ratio between the toroidal and poloidal magnetic fields, plasma surface area between the upper and lower null points at both inside and outside surfaces.

The toroidal magnetic field outside the plasma can be obtained by simply using $B_T \propto 1/R$, and the poloidal magnetic field can be calculated from poloidal flux by the following relation,

$$B_p = \frac{1}{R} |\nabla \Psi|.$$

The connection length and its poloidal projection can be obtained by

$$l = \int \sqrt{1 + \left(\frac{B_T}{B_p}\right)^2} \, dl_p \qquad \text{and} \qquad l_p = \int dl_p \; .$$

The integration should be carried out along flux surface in the poloidal direction.

Figure 4.2-1 explains notations which are used in this section. It should be noted that l_p, l, l_x and S_x correspond to the lengths and area between the median plane and null point, and that δ_x is a distance measured on the median plane between plasma surface and the flux surface on which above values are

evaluated. Three locations of the divertor plate are investigated, i.e., δ_x=50, 30 and 20 cm. In the poloidal plane, the divertor plates are represented as;

$$Z = 0.888R + 0.902 \quad m \qquad \delta x = 50 \quad cm,$$
$$Z = 0.888R + 0.467 \quad m \qquad \delta x = 30 \quad cm,$$
$$Z = 0.888R + 0.250 \quad m \qquad \delta x = 20 \quad cm.$$

Table 4.2-1 summarizes results for a plasma with β_p=1.0. If the divertor plate is placed at 20 cm apart from the null point, the ratio between B_T and B_p is larger than a hundred at the hitting point of the outside surface on the divertor plate. Such large values of B_T/B_p require quite accurate manufacturing and alignment of the divertor plate and management to avoid non-uniform or local heating of the plate. If the divertor plate is separated by 30 cm, the value of B_T/B_p becomes reasonable on the outside surface, but the value is still large on the inside surface. This is because of the larger toroidal magnetic field at the inside surface and of the existence of the divertor plate at expanded flux surface region. For δ_x smaller than 30 cm, divertor plate exists below the null point on the inside surface where flux surfaces are rather dense, B_T/B_p therefore decreases. Based on the above results, it is preferable to separate the divertor plate more than 30 cm from the null point.

Table 4.2-1 Summary of scrape-off layer quantities

(1) Outside Surface (ℓ_x = 45.5 m, S_x = 289 m²)

δ_M (cm)	δ_x = 50 cm			δ_x = 30 cm			δ_x = 20 cm		
	ℓ_p	ℓ	B_T/B_p	ℓ_p	ℓ	B_T/B_p	ℓ_p	ℓ	B_T/B_p
0.05	7.23	91.5	6.67	6.13	79.1	20.8	5.67	56.4	146
1	7.03	53.2	6.33	6.05	43.9	14.7	5.69	37.0	262
2	6.98	46.7	6.03	6.07	39.0	12.0	5.72	33.9	182
4	6.95	40.8	5.59	6.12	34.7	9.44	5.79	31.1	126

(2) Inside Surface (ℓ_x = 62.6 m, S_x = 119 m²)

δ_M (cm)	δ_x = 50 cm			δ_x = 30 cm			δ_x = 20 cm		
	ℓ_p	ℓ	B_T/B_p	ℓ_p	ℓ	B_T/B_p	ℓ_p	ℓ	B_T/B_p
0.05	5.10	99.6	23.5	4.75	86.6	65.4	4.56	49.7	148
1	4.90	54.0	22.9	4.56	43.3	45.1	4.37	34.8	37.9
2	4.81	47.2	21.9	4.48	37.9	43.1	4.28	31.6	27.5
4	4.69	40.9	20.2	4.35	33.1	24.8	4.15	28.5	20.4

Unit in ℓ_p and ℓ is meter

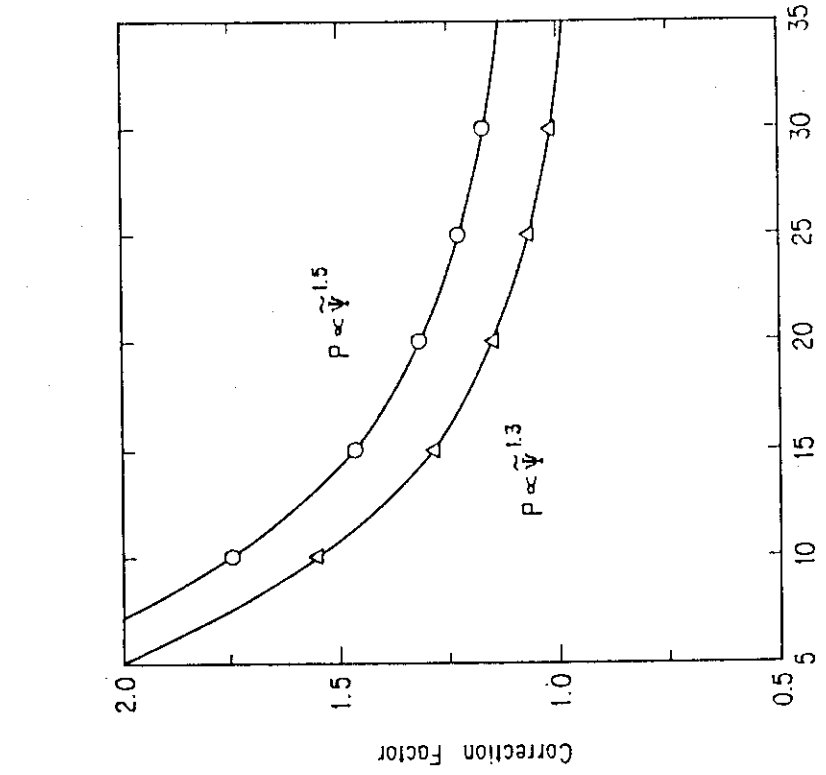

Fig. 4.1-2 Average ion temperature dependence of the correction factor for the fusion power output calculated from the average ion temperature and density.

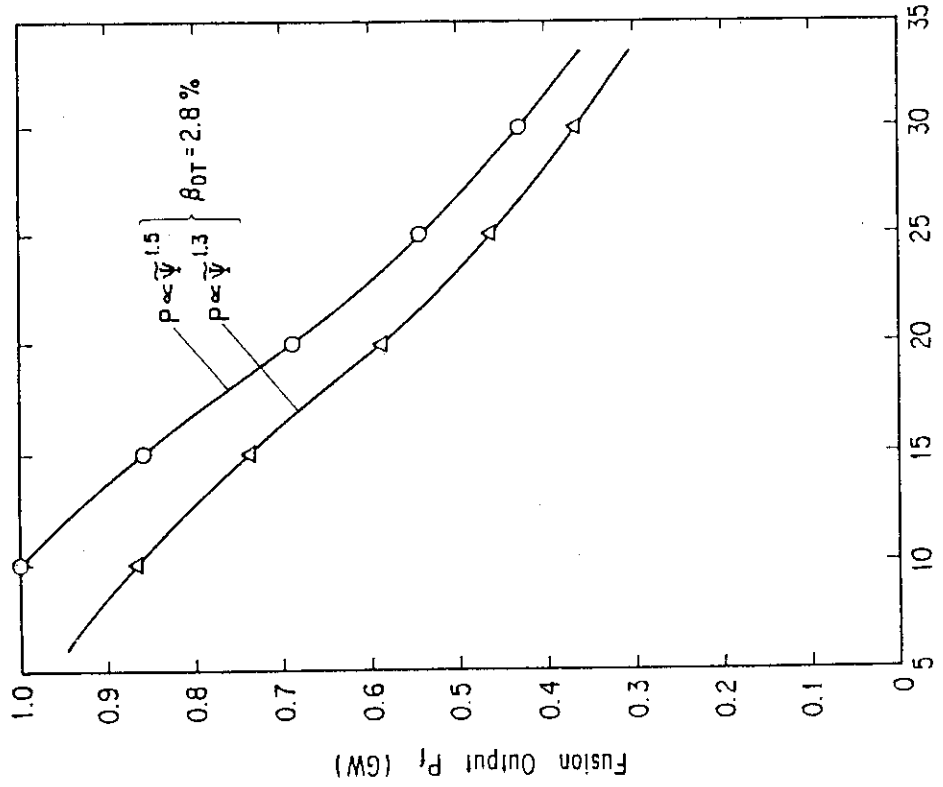

Fig. 4.1-1 Average ion temperature dependences of the fusion power output for different peaking of the plasma pressure. The average plasma pressure is kept constant.

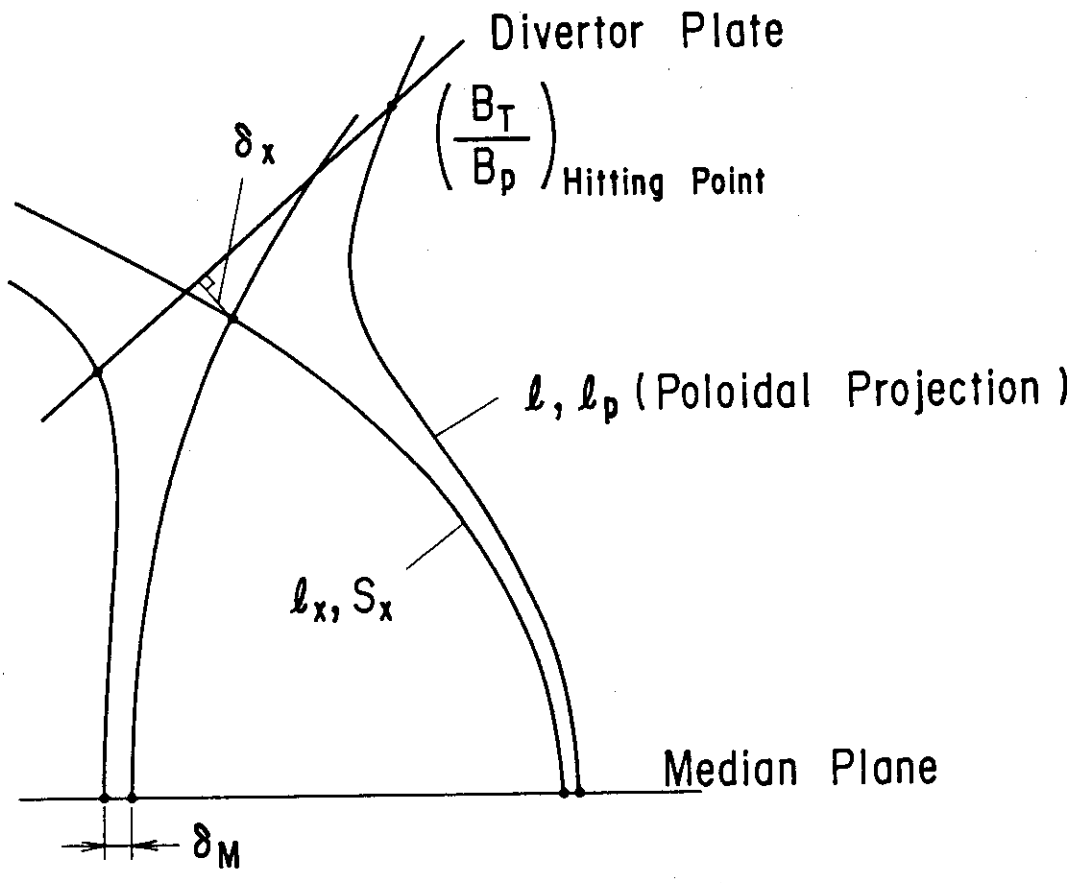

Fig. 4.2-1 Notations for calculating scrape-off layer quantities.

Acknowledgements

The authors wish to acknowledge Dr. K. Tomabechi, a chairman of the ITER Management Committee, for his continuous encouragement. Many thanks are due to Dr. Y. Shimomura for his leadership on the design work of the ITER basic device, in which our study was accomplished, and also for helpful advice and pointing on the direction of the study. Dr. M. Yamada gave us many useful informations about the ITER structure so that we could establish the concrete bases for the equilibrium analysis and optimization study. Thanks are also expressed to him.